Received: 5 May 2022 | Revised: 24 March 2023 | Accepted: 25 April 2023

DOI: 10.1002/num.23040

RESEARCH ARTICLE

WILEY

Virtual element method for elliptic bulk-surface PDEs in three space dimensions

Massimo Frittelli[1] | **Anotida Madzvamuse**[2] | **Ivonne Sgura**[1]

[1]Department of Mathematics and Physics "E. De Giorgi", University of Salento, Lecce, Italy
[2]Mathematics Department, The University of British Columbia, Vancouver, British Columbia, Canada

Correspondence
Massimo Frittelli, Department of Mathematics and Physics "E. De Giorgi," University of Salento, Lecce, 73100, Italy.
Email: massimo.frittelli@unisalento.it

Funding information
Engineering and Physical Sciences Research Council, Grant/Award Number: EP/T00410X/1; European Union NextGenerationEU - PNRR, Grant/Award Numbers: CN00000013, CUP F83C22000740001; Health Foundation, Grant/Award Number: 1902431; Istituto Nazionale di Alta Matematica "Francesco Severi", Grant/Award Number: CUP_E55F22000270001; Ministero dell'Università e della Ricerca - PRIN, Grant/Award Number: 2020F3NCPX; Natural Sciences and Engineering Research Council of Canada, Grant/Award Number: RGPIN-2023-05231; NIHR Biomedical Research Centre, Royal Marsden NHS Foundation Trust/Institute of Cancer Research, Grant/Award Number: NIHR133761; Regione Puglia, Grant/Award Number: UNISAL026, 901D2CAA.

Abstract

In this work we present a novel bulk-surface virtual element method (BSVEM) for the numerical approximation of elliptic bulk-surface partial differential equations in three space dimensions. The BSVEM is based on the discretization of the bulk domain into polyhedral elements with arbitrarily many faces. The polyhedral approximation of the bulk induces a polygonal approximation of the surface. We present a geometric error analysis of bulk-surface polyhedral meshes independent of the numerical method. Then, we show that BSVEM has optimal second-order convergence in space, provided the exact solution is $H^{2+3/4}$ in the bulk and H^2 on the surface, where the additional $\frac{3}{4}$ is due to the combined effect of surface curvature and polyhedral elements close to the boundary. We show that general polyhedra can be exploited to reduce the computational time of the matrix assembly. Two numerical examples on the unit sphere and on the Dupin ring cyclide confirm the convergence result.

KEYWORDS

bulk-surface PDEs, bulk-surface virtual element method, convergence analysis, polyhedral meshes

1 | INTRODUCTION

In this work, we introduce the bulk-surface virtual element method (BSVEM) for the numerical approximation of elliptic bulk-surface partial differential equations (BSPDEs) in three space dimensions (3D) of the following form:

$$\begin{cases} -\Delta u(\boldsymbol{x}) + u(\boldsymbol{x}) = f(\boldsymbol{x}), & \boldsymbol{x} \in \Omega; \\ -\Delta_\Gamma v(\boldsymbol{x}) + v(\boldsymbol{x}) + \nabla u(\boldsymbol{x}) \cdot \boldsymbol{\nu}(\boldsymbol{x}) = g(\boldsymbol{x}), & \boldsymbol{x} \in \Gamma; \\ \nabla u(\boldsymbol{x}) \cdot \boldsymbol{\nu}(\boldsymbol{x}) = -\alpha u(\boldsymbol{x}) + \beta v(\boldsymbol{x}), & \boldsymbol{x} \in \Gamma, \end{cases} \tag{1}$$

where $\Omega \subset \mathbb{R}^3$ is an open set such that $\Gamma = \partial\Omega$ is a smooth surface, Δ is the Laplace operator in Ω, Δ_Γ is the Laplace–Beltrami operator on Γ [32], $\boldsymbol{\nu}$ is the outward unit normal vector field on Γ, $\alpha, \beta > 0$, and $f : \Omega \to \mathbb{R}$ and $g : \Gamma \to \mathbb{R}$ are data. The problem (1) is taken from [33] and is the prototype of *coupled BSPDEs*, a class of problems that is recently drawing attention in the literature. More generally, given a number $d \in \mathbb{N}$ of space dimensions, a system of BSPDEs comprises of $m \in \mathbb{N}$ PDEs posed in the *bulk* $\Omega \subset \mathbb{R}^d$, coupled with $n \in \mathbb{N}$ PDEs posed on the surface $\Gamma := \partial\Omega$ through (i) either linear or non-linear coupling conditions [51], (ii) linear or nonlinear coupled kinetics [37] and possibly (iii) cross-diffusion [38]. The quickly growing interest toward stationary or time-dependent BSPDEs arises from the numerous applications of such PDE problems in different areas, such as cellular biological systems [27, 34, 50, 55], fluid dynamics [18, 22, 48], plant biology [56], biological patterning [36, 47], and electrochemistry [46] among many other applications.

Among the various state-of-the art numerical methods for the spatial discretization of BSPDEs existing in the literature we mention bulk-surface finite elements (BSFEM) [33, 45, 51, 52], trace finite elements [44], cut finite elements [22], discontinuous Galerkin methods [26], kernel collocation method [25], and closest point method [49].

The purpose of the present paper is to introduce a novel BSVEM of lowest polynomial degree $k = 1$ for the spatial discretization of elliptic BSPDEs in $d = 3$ space dimensions. The BSVEM is a substantial extension of the recently introduced virtual element method (VEM) for the numerical approximation of several classes of PDEs on flat domains [7] or surfaces [40]. The key feature of VEM is that of being a *polyhedral* method, that is, it handles elements of a quite general polyhedral shape, rather than just of tetrahedral shape [7]. The success of virtual elements is due to several advantages arising from polyhedral mesh generality, such as: (i) computationally cheap mesh pasting [16, 24, 40], (ii) efficient adaptive algorithms [23], (iii) flexible approximation of the domain and its boundary [28], (iv) nonconforming elements [43], and (iv) the possibility of enforcing higher regularity to the numerical solution [4, 13, 21]. Thanks to these advantages, several extensions of the original VEM for the Poisson equation [7] were developed for numerous PDE problems, such as heat [60] and wave equations [59], reaction-diffusion systems [1], Cahn–Hilliard equation [4], Stokes equation [12], Helmholtz equation [53], linear elasticity models [8], plate bending [21], fracture problems with geophysical applications [15, 41], eigenvalue problems [54] and many more.

On one hand, our proposed numerical methodology combines the VEM for the bulk equations [10] with the *surface virtual element method* (SVEM) [40] for the surface equations. On the other hand, the numerical method extends the two-dimensional BSVEM introduced in [35]. A marked difference with the work presented in [35] is that the surface PDEs were solved using the (one-dimensional) surface finite elements while, in this work, we employ virtual elements for both bulk and surface PDEs. Here, the method relies on an arbitrary polyhedral discretization of the bulk and its corresponding induced polygonal approximation of the surface. To the best of our knowledge, this kind of geometrical approximation is novel in the literature. In the special case of tetrahedral meshes, the method boils

down to the BSFEM [33, 52]. Since polyhedral meshes imply a geometric error in the approximation of curved boundaries, in this work we confine the BSVEM to the lowest polynomial degree $k = 1$ for the approximation space, when the geometric error does not dominate [30]. To formulate a higher order BSVEM it is then necessary to consider polyhedral elements with curved faces. However, the definition of a computable VEM function space on curved polygons and polyhedra is a challenging task that was addressed only in specific cases [5, 14, 29]. Furthermore, in our context, the coupled nature of the model problem (1) constrains the discrete function space on $\Gamma = \partial\Omega$ to be the trace of the discrete function space in Ω. A high order BSVEM that simultaneously fulfils all these properties is part of our current studies. The theoretical novelty of the present study is threefold:

1. We provide a geometric error analysis of polyhedral bulk-surface meshes that is independent of the numerical method and applies, in principle, to any method based on polyhedral bulk-surface meshes.
2. We carry out a full error analysis of the BSVEM. The proposed method possesses optimal second-order convergence provided the numerical solution is $H^{2+3/4}(\Omega)$ in the bulk instead of the usual requirement of $H^2(\Omega)$, see [33]. However, our analysis requires such extra regularity only in the simultaneous presence of a curved boundary Γ and non-tetrahedral elements close to the boundary, a novel case. We point out that such extra regularity comes for free in most models and applications, where the domains are smooth and the solutions are infinitely differentiable. To the best of the authors' knowledge, it remains an open problem to determine if such extra regularity is also a necessary condition.
3. In the case $\beta = 0$ in (1), the first equation in (1) becomes a bulk-only PDE with non-zero Neumann boundary conditions. Hence, a by-product of the proposed analysis is that *the lowest-order VEM for bulk-only elliptic PDEs in 3D retains optimal convergence in the simultaneous presence of a curved boundary* Γ, *non-tetrahedral elements close to* Γ, *and non-zero Neumann boundary data*. Interestingly enough, this problem was fully addressed only in specific cases. For example, in the simplest case (FEM on tetrahedral meshes), the result was proven in [6]. For the case of VEM on general polyhedral meshes, the seminal work [10] is confined to polyhedral domains. Then, in [14] and [29] the authors consider a VEM in 2D with curved edges and a VEM in 3D with curved faces, respectively, to take out the geometric error. In [17] the authors introduce a 2D VEM with suitable algebraic corrections that account for curved boundaries. The present work addresses the 3D setting and, to the best of the authors' knowledge, fills the theoretical gap on geometric error analysis for the bare-bone VEM for the lower order case.

In addition, we show that the usage of suitable polyhedra drastically reduces the computational time of matrix assembly on equal meshsize in comparison to the tetrahedral BSFEM. This property, which already holds true in the 2D case [35], is even more accentuated in 3D. Similar results are obtained in the literature through other methods, such as trace [44] or cut [22] finite elements. This property is particularly beneficial when matrix assembly takes the vast majority of the computational time, that is, for (i) time-independent problems [33] and (ii) time-dependent problems on evolving domains, where the matrices must be computed at each timestep [39].

The structure of our article is as follows. In Section 2, we derive the weak formulation of problem (1) and we state existence, uniqueness, and regularity results. In Section 3, we introduce polyhedral bulk-surface meshes and analyse the geometric error. In Section 4, we introduce the BSVEM for problem (1). In Section 5, we carry out the convergence analysis. In Section 6, we show that polyhedral meshes can significantly reduce the computational time of the matrix assembly. In Section 7, we provide two numerical examples to demonstrate: (i) polyhedral mesh generation on general geometries and (ii) the optimal convergence of the BSVEM. In Section 8, we state our conclusions and outline

future research directions. In Appendix A, we provide basic definitions and results required for the analysis.

2 | WEAK FORMULATION, EXISTENCE AND REGULARITY

To obtain the weak formulation of (1), we multiply the first two equations of (1) by two test functions $\alpha\varphi \in H^1(\Omega)$ and $\beta\psi \in H^1(\Gamma)$, respectively, then we apply Green's formula in the bulk Ω and on the curved manifold Γ [32], respectively. We obtain the following formulation: find $u \in H^1(\Omega)$ and $v \in H^1(\Gamma)$ such that

$$\begin{cases} \alpha \displaystyle\int_\Omega (\nabla u \cdot \nabla \varphi + u\varphi) = \alpha \int_\Omega f\varphi + \alpha \int_\Gamma \frac{\partial u}{\partial \boldsymbol{\nu}} \varphi; \\ \beta \displaystyle\int_\Gamma (\nabla_\Gamma v \cdot \nabla_\Gamma \psi + v\psi) + \beta \int_\Gamma \frac{\partial u}{\partial \boldsymbol{\nu}} \psi = \beta \int_\Gamma g\psi, \end{cases} \tag{2}$$

for all $\varphi \in H^1(\Omega)$ and $\psi \in H^1(\Gamma)$. By using the third equation of (1) in (2) and summing over the equations, we obtain the following weak formulation: find $(u, v) \in H^1(\Omega) \times H^1(\Gamma)$ such that

$$b((u, v); (\varphi, \psi)) = \alpha \int_\Omega f\varphi + \beta \int_\Gamma g\psi, \tag{3}$$

for all $(\varphi, \psi) \in H^1(\Omega) \times H^1(\Gamma)$, where $b((u, v); (\varphi, \psi)) : (H^1(\Omega) \times H^1(\Gamma))^2 \to \mathbb{R}$ is the bilinear form defined by

$$b((u, v); (\varphi, \psi)) = \alpha \int_\Omega (\nabla u \cdot \nabla \varphi + u\varphi) + \beta \int_\Gamma (\nabla_\Gamma v \cdot \nabla_\Gamma \psi + v\psi) + \int_\Gamma (\alpha u - \beta v)(\alpha\varphi - \beta\psi).$$

The variational formulation (3) fulfils the following result on existence, uniqueness and regularity found in [33].

Theorem 1 (Existence, uniqueness, and regularity [33]). *If Γ is a C^3 surface, $f \in L^2(\Omega)$ and $g \in L^2(\Gamma)$, the variational problem (3) has a unique solution $(u, v) \in H^2(\Omega) \times H^2(\Gamma)$ that fulfils the following bound*

$$\|(u, v)\|_{H^2(\Omega)\times H^2(\Gamma)} \leq C \|(f, g)\|_{L^2(\Omega)\times L^2(\Gamma)}. \tag{4}$$

Thanks to elliptic regularity, it is also possible to show that if $f \in H^1(\Omega)$ and $g \in H^1(\Omega)$, the regularity improves to

$$\|(u, v)\|_{H^3(\Omega)\times H^2(\Gamma)} \leq C \|(f, g)\|_{L^2(\Omega)\times L^2(\Gamma)}. \tag{5}$$

3 | GEOMETRIC ANALYSIS

In this section, we introduce bulk-surface polyhedral meshes and we analyse the geometric approximation error. The present analysis is independent of the numerical method and applies, in principle, to any polyhedral method for BSPDEs.

3.1 | Polyhedral bulk-surface meshes

Let $h > 0$ be a positive number called *meshsize* and let $\Omega_h = \cup_{E\in\mathcal{E}_h} E$ be a polyhedral approximation of the bulk Ω, where $\mathcal{E}_h$ is a set of non-degenerate compact polyhedra. The polyhedral bulk Ω_h automatically induces a polygonal approximation Γ_h of Γ, defined by $\Gamma_h = \partial\Omega_h$, exactly as in the case of

tetrahedral meshes, see [33]. Notice that we can write $\Gamma_h = \cup_{F\in\mathcal{F}_h} F$, where $\mathcal{F}_h$ is the set of the faces of Ω_h that constitute Γ_h. We assume that:

(F1) The diameter of each element $E \in \mathcal{E}_h$ does not exceed h;
(F2) For any two distinct elements or faces, their intersection is either empty, or a common vertex, or a common edge, or a common face.
(F3) All nodes of Γ_h lie on Γ;
(F4) Every face $F \in \mathcal{F}_h$ is contained in the Fermi stripe U of Γ (see Figure 1).
(V1) There exists $\gamma_1 > 0$ such that every $E \in \mathcal{E}_h$ and every face F of E is star-shaped with respect to a ball (with center x_E and x_F, respectively) of radius $\gamma_1 h_E$ and $\gamma_1 h_F$ respectively, where h_E and h_F are the diameters of E and F, respectively;
(V2) There exists $\gamma_2 > 0$ such that for all $E \in \mathcal{E}_h$ and for and every face F of E, the distance between any two nodes of E or F is at least $\gamma_2 h_E$ or $\gamma_2 h_F$, respectively.

Assumptions (F1)–(F4) are standard in the SFEM literature, see for instance [32], while Assumptions (V1) and (V2) are standard in the VEM literature, see for instance [7]. The combined Assumptions (F1)–(V2) will prove sufficient in our bulk-surface setting. In the following definitions and results, we provide the necessary theory for estimating the geometric error arising from the boundary approximation.

Definition 1 (Essentials of polyhedral bulk-surface meshes)**.** An element $E \in \mathcal{E}_h$ is called an exterior element if it has at least a face or an edge contained in Γ_h, otherwise E is called an interior element. Let Ω_B be the discrete narrow band defined as the union of the exterior elements of Ω_h as illustrated in Figure 1b. From Assumption (F4), for any face F contained in Γ_h we have that $\boldsymbol{a}(F) \subset \Gamma$, where $\boldsymbol{a}$ is the normal projection defined in Lemma 5.

Observe that, for sufficiently small $h > 0$, the discrete narrow band Ω_B is contained in the Fermi stripe U as shown in Figure 1b. Let $N \in \mathbb{N}$ and let $\boldsymbol{x}_i$, $i = 1, \dots, N$, be the nodes of Ω_h. Let $M \in \mathbb{N}$,

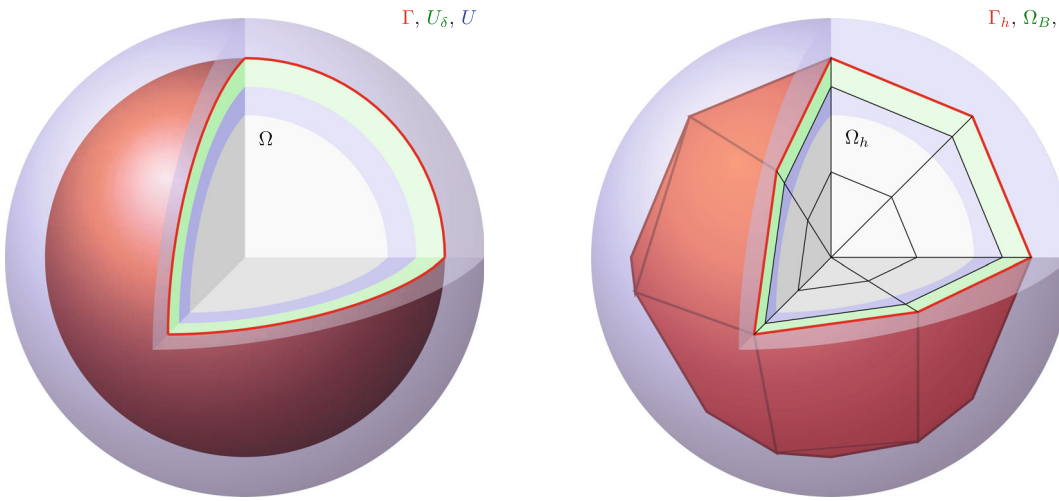

(a) Illustration of the *bulk* Ω enclosed by the *surface* Γ, the *narrow band* U_δ and the Fermi stripe U.

(b) Illustration of the *discrete bulk* Ω_h enclosed by the *discrete surface* Γ_h, the *discrete narrow band* Ω_B and the Fermi stripe U.

FIGURE 1 Illustration of the continuous domain, the discrete domain, and related notations.

$M < N$ and assume that the nodes of Γ_h are $\boldsymbol{x}_k$, $k = 1, \dots, M$, that is, the first M nodes of Ω_h. Throughout the article, we need the following *reduction matrix* $R \in \mathbb{R}^{N\times M}$ defined as $R := [I_M; 0]$, where I_M is the $M \times M$ identity matrix. The reduction matrix R fulfils the following two properties:

- For $\boldsymbol{v} \in \mathbb{R}^N$; $R^T\boldsymbol{v} \in \mathbb{R}^M$ is the vector with the first M entries of $\boldsymbol{v}$;
- For $\boldsymbol{w} \in \mathbb{R}^M$; $R\boldsymbol{w} \in \mathbb{R}^N$ is the vector whose first M entries are those of $\boldsymbol{w}$ and the other $N - M$ entries are 0.

In what follows, we will use the matrix R for an optimized implementation of the BSVEM.

3.2 | Variational crime

We now consider the geometric error due to the boundary approximation. Since the surface variational crime in surface virtual elements is well-understood [40], we will mainly focus on the variational crime in the bulk. To this end, it is useful to analyse the relation between any element $E \in \mathcal{E}_h$ and a suitably defined *exact element* $\breve{E}$ (a curved version of E), see Figure 2 for an illustration. For the special case of tetrahedral meshes with at most one boundary face per element, $\breve{E}$ is rigorously defined and there exists a C^2 mapping with C^2 inverse between E and $\breve{E}$. Such mapping is linearly close to the identity with respect to the meshsize, see [33]. In the more general case when E has more than four faces and/or multiple boundary faces, we will show the existence of a mapping between E and a suitably defined $\breve{E}$ with slightly weaker regularity, which is sufficient for our purposes.

Lemma 1 (Domain parametrization)**.** *Let $\mathcal{E}_h$ fulfil assumptions (F1)–(V2). There exists a homeomorphism $G : \Omega_h \to \Omega$ such that $G \in W^{1,\infty}(\Omega_h)$ and*

$$G|_{\Gamma_h} = \boldsymbol{a}|_{\Gamma_h}; \tag{6}$$

$$G|_{\Omega_h\setminus\Omega_B} = I; \tag{7}$$

$$\|J_G - I\|_{L^\infty(\Omega_B)} \le Ch; \tag{8}$$

$$\|\det(J_G) - 1\|_{L^\infty(\Omega_B)} \le Ch; \tag{9}$$

$$\|G - I\|_{L^\infty(\Omega_B)} \le Ch^2, \tag{10}$$

where $\boldsymbol{a}$ is the normal projection defined in Lemma 5 in the Appendix, J_G is the Jacobian of G, $C > 0$ is a constant that depends on Γ, the constants γ_1, γ_2 are those considered in Assumptions (V1) and (V2), and I is the identity matrix. Even if restricted to a single element $E \in \mathcal{E}_h$, G might not be C^2 (not even C^1) unless E is a tetrahedron.

Proof. Consider a bulk element $E \in \mathcal{E}_h$ and assume that all of the faces of E that are contained in Γ_h are also in the Fermi stripe U, see Figure 2a. Pick a face F of E and let x_E and x_F be as in Assumption (V1). By joining x_E and x_F with the midpoints of two consecutive edges of F, a tetrahedron T is obtained, see Figure 2b. By proceeding in this fashion, E can be subdivided into a finite amount N_E of tetrahedra $T_1, \dots, T_{N_E}$ that are quasi-uniform thanks to the geometric assumptions (V1) and (V2). Then, replace each T_i by its exact (curved) counterpart $\breve{T}_i$ as defined in [33], see Figure 2c. The exact element $\breve{E}$ is then defined by replacing each T_i by its curved counterpart $\breve{T}_i$, see Figure 2d. The

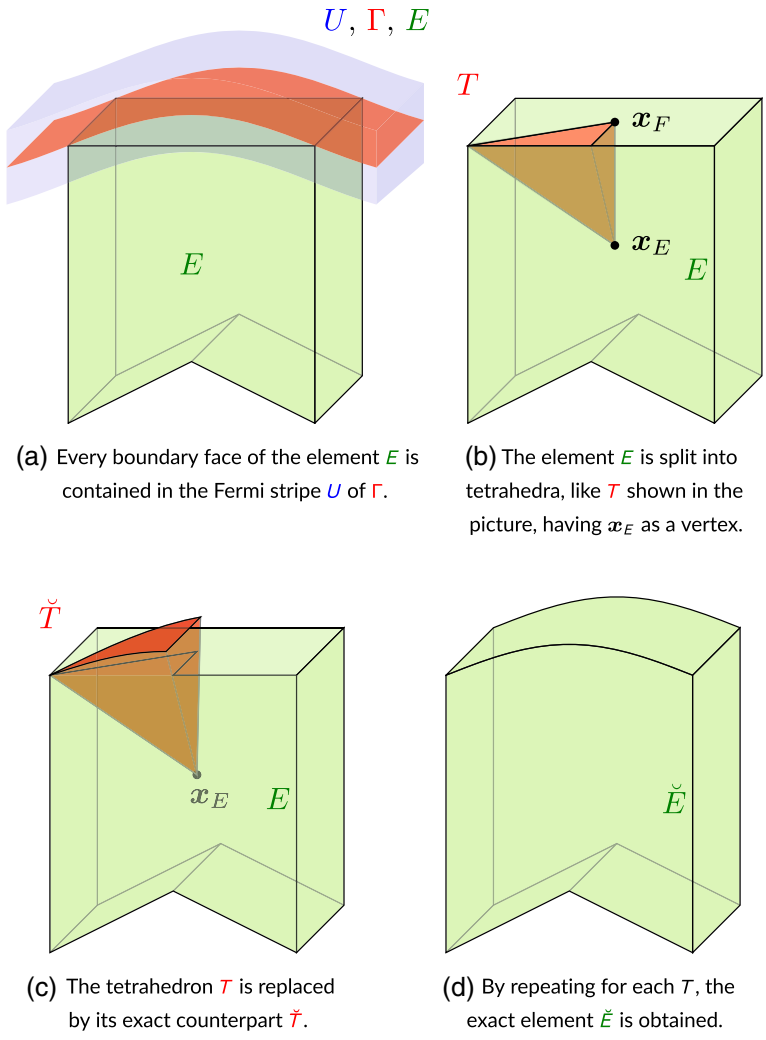

(a) Every boundary face of the element E is contained in the Fermi stripe U of Γ.

(b) The element E is split into tetrahedra, like T shown in the picture, having $\boldsymbol{x}_E$ as a vertex.

(c) The tetrahedron T is replaced by its exact counterpart $\check{T}$.

(d) By repeating for each T, the exact element $\check{E}$ is obtained.

FIGURE 2 Steps of the construction of the exact element $\check{E}$ corresponding to a given element E, following Lemma 1. The symbols U, Γ, E are color-matched with the figure.

claimed map G is constructed piecewise by applying [33, Proposition 4.7] for all the T_i's of each $E \in \mathcal{E}_h$. If restricted to a single T_i, the map G is C^2 [33, Lemma 4.6]. ∎

Thanks to Lemma 1, it is possible to define bulk- and surface-lifting operators.

Definition 2 (Bulk- and surface-lifting operators)**.** Given $V : \Omega_h \to \mathbb{R}$ and $W : \Gamma_h \to \mathbb{R}$, their lifts are defined by $V^\ell := V \circ G^{-1}$ and $W^\ell := W \circ G^{-1}$, respectively. Conversely, given $v : \Omega \to \mathbb{R}$ and $w : \Gamma \to \mathbb{R}$, their inverse lifts are defined by $v^{-\ell} := v \circ G$ and $w^{-\ell} := w \circ G$, respectively, with $G : \Omega_h \to \Omega$ being the mapping defined in Lemma 1.

Lemma 1 also enables us to show the equivalence of Sobolev norms under lifting as illustrated next.

Lemma 2 (Equivalence of norms under lifting)**.** *There exists two constants $c_2 > c_1 > 0$ depending on Γ and γ_2 such that, for all $V : \Omega_h \to \mathbb{R}$ and for all $W : \Gamma_h \to \mathbb{R}$,*

$$c_1 \|V^\ell\|_{L^2(\Omega)} \leq \|V\|_{L^2(\Omega_h)} \leq c_2 \|V^\ell\|_{L^2(\Omega)}; \tag{11}$$

$$c_1|V^\ell|_{H^1(\Omega)} \leq |V|_{H^1(\Omega_h)} \leq c_2|V^\ell|_{H^1(\Omega)}; \tag{12}$$

$$c_1\|W^\ell\|_{L^2(\Gamma)} \leq \|W\|_{L^2(\Gamma_h)} \leq c_2\|W^\ell\|_{L^2(\Gamma)}; \tag{13}$$

$$c_1|W^\ell|_{H^1(\Gamma)} \leq |W|_{H^1(\Gamma_h)} \leq c_2|W^\ell|_{H^1(\Gamma)}; \tag{14}$$

$$|W|_{H^2(\Gamma_h)} \leq c_2|W^\ell|_{H^2(\Gamma)} + c_2h|W^\ell|_{H^1(\Gamma)}. \tag{15}$$

Proof. Estimates (11) and (12) follow by using the map G introduced in Lemma 1 in the proof of [33, Proposition 4.9]. A proof of (13)–(15) is in [32, Lemma 4.2]. ∎

We are ready to estimate the effect of lifting on bulk- and surface integrals.

Lemma 3 (Geometric error of lifting)**.** *If* $u, \varphi \in H^1(\Omega)$, *then*

$$\left|\int_\Omega \nabla u \cdot \nabla\varphi - \int_{\Omega_h} \nabla u^{-\ell} \cdot \nabla\varphi^{-\ell}\right| \leq Ch|u|_{H^1(\Omega_B^\ell)}|\varphi|_{H^1(\Omega_B^\ell)}, \tag{16}$$

$$\left|\int_\Omega u\varphi - \int_{\Omega_h} u^{-\ell}\varphi^{-\ell}\right| \leq Ch\|u\|_{L^2(\Omega_B^\ell)}\|\varphi\|_{L^2(\Omega_B^\ell)}, \tag{17}$$

where $C > 0$ *depends on* Γ, γ_1 *and* γ_2. *If* $v, \psi \in H^1(\Gamma)$, *then*

$$\left|\int_\Gamma \nabla_\Gamma v \cdot \nabla_\Gamma\psi - \int_{\Gamma_h} \nabla_{\Gamma_h} v^{-\ell} \cdot \nabla_{\Gamma_h}\psi^{-\ell}\right| \leq Ch^2|v|_{H^1(\Gamma)}|\psi|_{H^1(\Gamma)}; \tag{18}$$

$$\left|\int_\Gamma v\psi - \int_{\Gamma_h} v^{-\ell}\psi^{-\ell}\right| \leq Ch^2\|v\|_{L^2(\Gamma)}\|\psi\|_{L^2(\Gamma)}, \tag{19}$$

where $C > 0$ *depends on* Γ, γ_1 *and* γ_2.

Proof. To prove (16) and (17) it suffices to use the bulk geometric estimates (7)–(9) in the proof of [33, Lemma 6.2]. A proof of (18) and (19) can be found in [32]. ∎

Remark 1 (Polyhedral meshes and curved boundaries)**.** From Lemma 1, we know that G might not be a C^2 mapping with C^2 inverse in the simultaneous presence of general polyhedral elements and curved boundaries. This issue does not arise in the absence of curved boundaries [10], when G is the identity by construction, nor in the absence of non-tetrahedral elements [45]. This implies that, in the simultaneous presence of curved boundaries and non-tetrahedral elements, the lifting operator does not preserve the Sobolev regularity of functions. That is to say, for $E \in \mathcal{E}_h$ the inverse lift of an $H^2(\check{E})$ function is not, in general, $H^2(E)$. Now, since our analysis requires full regularity of the exact solution mapped on the polyhedral domain, we need an alternative mapping instead of the lifting. Hence, we consider the Sobolev extension.

Lemma 4 (Geometric error of Sobolev extension)**.** *There exist* $C > 0$ *such that*

$$\|\widetilde{u} - u^{-\ell}\|_{L^2(\Omega_h)} \leq Ch^2\|u\|_{H^{2+1/4}(\Omega)}, \quad \forall\, u \in H^{2+1/4}(\Omega); \tag{20}$$

$$|\widetilde{u} - u^{-\ell}|_{H^1(\Omega_h)} \leq Ch^{\frac{3}{2}}\|u\|_{H^2(\Omega)} + Ch\|u\|_{H^{2+3/4}(\Omega)}, \quad \forall\, u \in H^{2+1/4}(\Omega), \tag{21}$$

where $\widetilde{u}$ *denotes the Sobolev extension of* u, *defined in Theorem 7*.

Proof. By using (A6), (A7) in Appendix A with $\gamma = \frac{3}{4}$, (7) and (10) we have that

$$\begin{aligned}
\|\widetilde{u} - u^{-\ell}\|_{L^2(\Omega_h)} &= \|\widetilde{u} - \widetilde{u} \circ G\|_{L^2(\Omega_h)} \leq C\|\widetilde{u}\|_{H^{3/2+3/4}(\Omega_h)}\|(I-G)^{3/4}\|_{L^2(\Omega_h)} \\
C\|u\|_{H^{3/2+3/4}(\Omega)}\|(I-G)^{3/4}\|_{L^2(\Omega_B)} &\leq C\|u\|_{H^{3/2+3/4}(\Omega)}|\Omega_B|^{1/2}\|I-G\|^{3/4}_{L^\infty(\Omega_B)} \\
&\leq Ch^{\frac{1}{2}}h^{\frac{3}{2}}\|u\|_{H^{3/2+3/4}(\Omega)} = Ch^2\|u\|_{H^{2+1/4}(\Omega)}, \qquad (22)
\end{aligned}$$

which proves (20). Notice that, in the last line of (22), the $h^{\frac{1}{2}}$ term is the effect of the Sobolev extension being exact except on the discrete narrow band Ω_B. Using (8), (10), and (A3), (A6) in Appendix A, we have that

$$\begin{aligned}
|\widetilde{u} - u^{-\ell}|_{H^1(\Omega_h)} &= \|\nabla\widetilde{u} - (J_G^T\,\nabla\widetilde{u}) \circ G\|_{L^2(\Omega_h)} \leq \qquad (23) \\
\|(I - J_G^T \circ G)\|_{L^\infty(\Omega_h)}\|\nabla\widetilde{u}\|_{L^2(\Omega_B)} &+ \|J_G^T \circ G\|_{L^\infty(\Omega_h)}\|\nabla\widetilde{u} - \nabla\widetilde{u} \circ G\|_{L^2(\Omega_h)} \leq \\
Ch\|\nabla\widetilde{u}\|_{L^2(\Omega_B)} + C\|\nabla\widetilde{u} - \nabla\widetilde{u} \circ G\|_{L^2(\Omega_h)} &\leq Ch^{\frac{3}{2}}\|u\|_{H^2(\Omega)} + C\|\nabla\widetilde{u} - \nabla\widetilde{u} \circ G\|_{L^2(\Omega_h)}.
\end{aligned}$$

Since $\widetilde{u} \in H^{2+1/2+\gamma}(\Omega_h)$, then $\nabla\widetilde{u} \in H^{1+1/2+\gamma}(\Omega_h)$. Hence, by reasoning as in (22) we have that

$$\|\nabla\widetilde{u} - \nabla\widetilde{u} \circ G\|_{L^2(\Omega_h)} \leq C_\gamma h^{\frac{1}{2}+2\gamma}\|u\|_{H^{2+1/2+\gamma}(\Omega)}. \qquad (24)$$

By substituting (24) into (23) we get the desired estimate. ∎

4 | THE BULK-SURFACE VIRTUAL ELEMENT METHOD

In this section, we introduce the BSVEM for problem (1).

4.1 | Virtual element space on polygons and polyhedra

We start by defining virtual element spaces on polygons and polyhedra by following [10], but we simplify the presentation, as the present work is confined to first-degree elements. We start from the two dimensional spaces. Let F be a polygon that, without loss of generality, lies in $\mathbb{R}^2$. A preliminary virtual element space on F is given by

$$\widetilde{\mathbb{V}}(F) := \left\{ v \in H^1(F) \cap C^0(F) \,\middle|\, v_{|e} \in \mathbb{P}_1(e),\ \forall\, e \in \text{edges}(F) \wedge \Delta v \in \mathbb{P}_1(F) \right\}, \qquad (25)$$

where $\mathbb{P}_1(F)$ is the space of linear polynomials on the polygon F. Let us consider the elliptic projection $\Pi_F^\nabla : \widetilde{\mathbb{V}}(F) \to \mathbb{P}_1(F)$ defined by

$$\int_F \nabla(v - \Pi_F^\nabla v) \cdot \nabla p_1 = 0 \qquad \forall\, p_1 \in \mathbb{P}_1(F) \quad \wedge \quad \int_{\partial F} (v - \Pi_F^\nabla v) = 0. \qquad (26)$$

Thanks to Green's formula, the operator Π_F^∇ is computable, see [3] for the details. The so-called *enhanced virtual element space* in two dimensions is now defined as follows:

$$\mathbb{V}(F) := \left\{ v \in \widetilde{\mathbb{V}}(F) \,\middle|\, \int_F v p_1 = \int_F (\Pi_F^\nabla v) p_1,\ \forall\, p_1 \in \mathbb{P}_1(F) \right\}. \qquad (27)$$

For the three dimensional spaces, let now E be a polyhedron. The *boundary space* on ∂E and the preliminary virtual element space on E are defined by

$$\mathcal{B}(\partial E) = \{ v \in C^0(\partial E) | v_{|F} \in \mathbb{V}(F),\ \forall F \in \text{faces}(E) \};$$

$$\widetilde{\mathbb{V}}(E) := \left\{ v \in H^1(E) \,\middle|\, v_{|\partial E} \in \mathcal{B}(\partial E) \wedge \Delta v \in \mathbb{P}_1(E) \right\},$$

where $\mathbb{P}_1(E)$ is the space of linear polynomials on the polyhedron E. Let us consider the elliptic projection $\Pi_E^\nabla : \widetilde{\mathbb{V}}(E) \to \mathbb{P}_1(E)$ defined by

$$\int_E \nabla(v - \Pi_E^\nabla v) \cdot \nabla p_1 = 0 \qquad \forall\, p_1 \in \mathbb{P}_1(E) \quad \wedge \quad \int_{\partial E} (v - \Pi_E^\nabla v) = 0. \tag{28}$$

Once again, the operator Π_E^∇ is computable, see [3] for the details. The enhanced virtual element space in 3D is now defined as follows:

$$\mathbb{V}(E) := \left\{ v \in \widetilde{\mathbb{V}}(E) \,\middle|\, \int_E v p_1 = \int_E (\Pi_E^\nabla v) p_1,\ \forall\, p_1 \in \mathbb{P}_1(E) \right\}. \tag{29}$$

The practical usability of the spaces $\mathbb{V}(F)$ and $\mathbb{V}(E)$ stem from the following result.

Proposition 1 (Degrees of freedom [3]). *Let $n \in \mathbb{N}$. If E is a polygon or a polyhedron with n vertexes $\boldsymbol{x}_i$, $i = 1, \dots, n$, then $\dim(\mathbb{V}(E)) = n$ and each function $v \in \mathbb{V}(E)$ is uniquely defined by the nodal values $v(\boldsymbol{x}_i)$, $i = 1, \dots, n$. Hence, the nodal values constitute a set of degrees of freedom.*

The following definition allows to correctly handle functions that are multiply defined on the junction between elements.

Definition 3 (Broken Sobolev norms). Given two collections of functions $\{u_E : E \to \mathbb{R} | E \in \mathcal{E}_h\}$ and $\{v_F : F \to \mathbb{R} | F \in \mathcal{F}_h\}$, the broken Sobolev seminorms are defined as follows:

$$|u|_{s,\Omega,h} := \left(\sum_{E \in \mathcal{E}_h} |u_E|^2_{H^s(E)} \right)^{\frac{1}{2}}, \quad \text{and} \quad |v|_{s,\Gamma,h} := \left(\sum_{F \in \mathcal{F}_h} |v_F|^2_{H^s(F)} \right)^{\frac{1}{2}}, \qquad s = 1, 2.$$

Technical estimates for polynomial interpolation on polygons and polyhedra are given in the following result.

Proposition 2 (Projection error on polynomials [19]). *For $s = 1, 2$, given two collections of functions $\{u_E \in H^s(E) | E \in \mathcal{E}_h\}$ and $\{v_F \in H^s(F) | F \in \mathcal{F}_h\}$, there exist $u_\pi \in \prod_{E \in \mathcal{E}_h} \mathbb{P}_1(E)$ and $v_\pi \in \prod_{F \in \mathcal{F}_h} \mathbb{P}_1(F)$ such that*

$$\|u - u_\pi\|_{0,\Omega,h} + h|u - u_\pi|_{1,\Omega,h} \le Ch^s |u|_{s,\Omega,h}; \tag{30}$$

$$\|v - v_\pi\|_{0,\Gamma,h} + h|v - v_\pi|_{1,\Gamma,h} \le Ch^s |v|_{s,\Gamma,h}, \tag{31}$$

where $C > 0$ is a constant that depends only on γ_1.

The *global virtual element spaces* in the bulk and on the surface are defined by matching of degrees of freedom across elements:

$$\mathbb{V}_\Omega := \{ v \in H^1(\Omega_h) \mid v_{|E} \in \mathbb{V}(E),\ \forall\, E \in \mathcal{E}_h \}; \tag{32}$$

$$\mathbb{V}_\Gamma := \{ v \in C^0(\Gamma_h) \mid v_{|F} \in \mathbb{V}(F),\ \forall\, F \in \mathcal{F}_h \}. \tag{33}$$

In the global spaces $\mathbb{V}_\Gamma$ and $\mathbb{V}_\Omega$ we consider the Lagrange basis functions $\varphi_i \in \mathbb{V}_\Omega$ for $i = 1, \dots, N$ and $\psi_{i'} \in \mathbb{V}_\Gamma$ for $i' = 1, \dots, M$, where each φ_i and each $\psi_{i'}$ are uniquely defined by $\varphi_i(\boldsymbol{x}_j) = \delta_{ij}$ for all $i, j = 1, \dots, N$ and $\psi_{i'}(\boldsymbol{x}_{j'}) = \delta_{i'j'}$ for all $i', j' = 1, \dots, M$, respectively, with δ_{ij} being the Kronecker

symbol. The sets $\{\varphi_i,\ i = 1, \dots, N\}$ and $\{\psi_{i'},\ i' = 1, \dots, M\}$ are bases of $\mathbb{V}_\Omega$ and $\mathbb{V}_\Gamma$, respectively, thanks to Proposition 1. It is easy to see that the bulk- and surface-Lagrange basis functions fulfil the following relation:

$$\varphi_{i|\Gamma_h} = \psi_i, \qquad \forall\ i = 1, \dots, M. \tag{34}$$

4.2 | Approximation of bilinear forms

In order to derive a spatially discrete formulation of the weak continuous problem (3) we need suitable approximate bilinear forms. We will follow [3, 7]. In the remainder of this section, let F and E be elements of Γ_h and Ω_h, respectively. The *stabilizing forms* $S_F : \mathbb{V}(F) \times \mathbb{V}(F) \to \mathbb{R}$ and $S_E : \mathbb{V}(E) \times \mathbb{V}(E) \to \mathbb{R}$ are defined by

$$S_F(v, w) := \sum_{P \in \text{ vertexes } (F)} v(P)w(P), \qquad \forall\ v,\ w \in \mathbb{V}(F); \tag{35}$$

$$S_E(v, w) := \sum_{P \in \text{ vertexes } (E)} v(P)w(P), \qquad \forall\ v,\ w \in \mathbb{V}(E), \tag{36}$$

respectively. The L^2 projectors $\Pi^0_F : \mathbb{V}(F) \to \mathbb{P}_1(F)$ and $\Pi^0_E : \mathbb{V}(E) \to \mathbb{P}_1(E)$ are defined as follows: for $v \in \mathbb{V}(F)$ and $w \in \mathbb{V}(E)$:

$$\int_F (v - \Pi^0_F v)p = 0, \qquad \forall p \in \mathbb{P}_1(F); \tag{37}$$

$$\int_E (w - \Pi^0_E w)p = 0, \qquad \forall p \in \mathbb{P}_1(E), \tag{38}$$

respectively. As shown in [3], Π^0_F and Π^0_E are computable because $\Pi^0_F = \Pi^\nabla_F$ and $\Pi^0_E = \Pi^\nabla_E$. Even if Π^0_F and Π^0_E are not new projectors, the presentation and the analysis of the method benefit from the usage of the equivalent definitions (37) and (38). Moreover, since $\Pi^0_F = \Pi^\nabla_F$ and $\Pi^0_E = \Pi^\nabla_E$, the boundedness property of projection operators in Hilbert spaces translates to

$$\|\Pi^0_F v\|_{L^2(F)} \le \|v\|_{L^2(F)} \quad \text{and} \qquad |\Pi^0_F v|_{H^1(F)} \le |v|_{H^1(F)}; \tag{39}$$

$$\|\Pi^0_E w\|_{L^2(E)} \le \|w\|_{L^2(E)} \quad \text{and} \qquad |\Pi^0_E w|_{H^1(E)} \le |w|_{H^1(E)}. \tag{40}$$

We are now ready to introduce the approximate L^2 bilinear forms $m_F : \mathbb{V}(F) \times \mathbb{V}(F) \to \mathbb{R}$ and $m_E : \mathbb{V}(E) \times \mathbb{V}(E) \to \mathbb{R}$, defined as follows:

$$m_F(v, w) := \int_F (\Pi^0_F v)(\Pi^0_F w) + \text{area}(F) S_F(v - \Pi^0_F v, w - \Pi^0_F w); \tag{41}$$

$$m_E(v, w) := \int_E (\Pi^0_E v)(\Pi^0_E w) + \text{volume}(E) S_E(v - \Pi^0_E v, w - \Pi^0_E w), \tag{42}$$

respectively. The approximate gradient-gradient bilinear forms $a_F : \mathbb{V}(F) \times \mathbb{V}(F) \to \mathbb{R}$ and $a_E : \mathbb{V}(E) \times \mathbb{V}(E) \to \mathbb{R}$ are defined by

$$a_F(v, w) := \int_F (\nabla \Pi^\nabla_F v) \cdot (\nabla \Pi^\nabla_F w) + S_F(v - \Pi^\nabla_F v, w - \Pi^\nabla_F w); \tag{43}$$

$$a_E(v, w) := \int_E (\nabla \Pi^\nabla_E v) \cdot (\nabla \Pi^\nabla_E w) + \text{diam}(E) S_E(v - \Pi^\nabla_E v, w - \Pi^\nabla_E w), \tag{44}$$

respectively. The definitions of a_E, a_F, m_E, and m_F imply the following result.

Proposition 3 (Stability and consistency [11, 20]). *The bilinear forms a_E, a_F, m_E, and m_F are consistent, that is,*

$$a_F(v,p) = \int_F \nabla v \cdot \nabla p; \quad m_F(v,p) = \int_F vp, \qquad \forall p \in \mathbb{P}_1(F); \tag{45}$$

$$a_E(v,p) = \int_E \nabla v \cdot \nabla p; \quad m_E(v,p) = \int_E vp, \qquad \forall p \in \mathbb{P}_1(E). \tag{46}$$

The bilinear forms a_E, a_F, m_E, and m_F are stable, meaning that there exist two constants $0 < \alpha_* < \alpha^*$ depending on γ_2 such that, for all $v \in \mathbb{V}(F)$ and $w \in \mathbb{V}(E)$

$$\alpha_* \int_F \nabla v \cdot \nabla v \le a_F(v,v) \le \alpha^* \int_F \nabla v \cdot \nabla v; \quad \alpha_* \int_F v^2 \le m_F(v,v) \le \alpha^* \int_F v^2; \tag{47}$$

$$\alpha_* \int_E \nabla w \cdot \nabla w \le a_E(w,w) \le \alpha^* \int_E \nabla w \cdot \nabla w; \quad \alpha_* \int_E w^2 \le m_E(w,w) \le \alpha^* \int_E w^2. \tag{48}$$

We observe from (47) and (48) that the approximate bilinear forms a_E, a_F, m_E, and m_F do not converge to their exact counterparts, see also [7]. Nevertheless, we will show that the method retains optimal convergence thanks to the consistency properties (45) and (46). The global bilinear forms $a_h^\Gamma, m_h^\Gamma : \mathbb{V}_\Gamma \times \mathbb{V}_\Gamma \to \mathbb{R}$, and $a_h^\Omega, m_h^\Omega : \mathbb{V}_\Omega \times \mathbb{V}_\Omega \to \mathbb{R}$ are defined elementwise:

$$a_h^\Gamma(v,w) := \sum_{F \in \mathcal{F}_h} a_F(v_{|F}, w_{|F}); \quad m_h^\Gamma(v,w) := \sum_{F \in \mathcal{F}_h} m_F(v_{|F}, w_{|F}); \tag{49}$$

$$a_h^\Omega(v,w) := \sum_{E \in \mathcal{E}_h} a_E(v_{|E}, w_{|E}); \quad m_h^\Omega(v,w) := \sum_{E \in \mathcal{E}_h} m_E(v_{|E}, w_{|E}). \tag{50}$$

From Proposition 3, m_h^Γ and m_h^Ω are positive definite, while a_h^Γ and a_h^Ω are positive semi-definite.

4.3 | Approximation of the load terms

The approximate bilinear forms m_h^Γ and m_h^Ω presented in the previous section are not sufficient to discretize load terms like $\int_\Gamma g\varphi$ and $\int_\Omega f\varphi$, because g and f are not in the spaces $\mathbb{V}_\Gamma$ and $\mathbb{V}_\Omega$, respectively.

Definition 4 (Surface- and bulk-virtual Lagrange interpolants). Given $f \in C^0(E)$, $E \in \mathcal{E}_h$ and $g \in C^0(F)$, $F \in \mathcal{F}_h$, the virtual Lagrange interpolants $I_E(f)$ of f and $I_F(g)$ of g are the unique $\mathbb{V}(E)$ and $\mathbb{V}(F)$ functions, respectively, such that $I_E(f)(\boldsymbol{x}) = f(\boldsymbol{x})$ for all $\boldsymbol{x} \in$ vertexes(E) and $I_F(g)(\boldsymbol{x}) = g(\boldsymbol{x})$ for all $\boldsymbol{x} \in$ vertexes(F), respectively. Given two collections of functions $\{f_E \in C^0(E) | E \in \mathcal{E}_h\}$ and $\{g_F \in C^0(F) | F \in \mathcal{F}_h\}$, their global interpolants are the collections of functions defined by $I_\Omega(f) = \{I_E(f_E) | E \in \mathcal{E}_h\}$ and $I_\Gamma(g) = \{I_F(g_F) | F \in \mathcal{F}_h\}$.

Proposition 4 (Interpolation error [20]). *Given two collections of functions $\{f_E \in H^2(E) | E \in \mathcal{E}_h\}$ and $\{g_F \in H^2(F) | F \in \mathcal{F}_h\}$, it holds that*

$$\|f - I_\Omega(f)\|_{L^2(\Omega_h)} + h|f - I_\Omega(f)|_{1,\Omega,h} \le Ch^2 |f|_{2,\Omega,h}; \tag{51}$$

$$\|g - I_\Gamma(g)\|_{L^2(\Gamma_h)} + h|g - I_\Gamma(g)|_{1,\Gamma,h} \le Ch^2 |g|_{2,\Gamma,h}, \tag{52}$$

respectively, where $C > 0$ depends only on γ_1.

4.4 | The spatially discrete formulation

The discrete counterpart of the weak elliptic problem (3) is: find $(U, V) \in \mathbb{V}_\Omega \times \mathbb{V}_\Gamma$ such that

$$b_h((U,V);(\varphi,\psi)) = \alpha m_h^\Omega(I_\Omega(f),\varphi) + \beta m_h^\Gamma(I_\Gamma(g),\psi), \quad \forall (\varphi,\psi) \in \mathbb{V}_\Omega \times \mathbb{V}_\Gamma, \tag{53}$$

where $b_h : (\mathbb{V}_\Omega \times \mathbb{V}_\Gamma)^2 \to \mathbb{R}$ is the discrete bilinear form defined by

$$b_h((U,V);(\varphi,\psi)) := \alpha \left(a_h^\Omega(U,\varphi) + m_h^\Omega(U,\varphi)\right) + \beta \left(a_h^\Gamma(V,\psi) + m_h^\Gamma(V,\psi)\right) + m_h^\Gamma(\alpha U - \beta V, \alpha\varphi - \beta\psi). \tag{54}$$

The discrete formulation (53) is suitable for the theoretical error analysis. We now derive an equivalent formulation of the discrete problem (53) that is suitable for the implementation. To this end, we express the spatially discrete solution (U, V) in the Lagrange bases as follows:

$$U(\boldsymbol{x}) = \sum_{i=1}^{N} \xi_i \varphi_i(\boldsymbol{x}), \qquad \boldsymbol{x} \in \Omega_h; \quad \text{and} \quad V(\boldsymbol{x}) = \sum_{k=1}^{M} \eta_k \psi_k(\boldsymbol{x}), \qquad \boldsymbol{x} \in \Gamma_h. \tag{55}$$

Hence, problem (53) is equivalent to: find $\boldsymbol{\xi} := (\xi_i, \dots, \xi_N)^T \in \mathbb{R}^N$ and $\boldsymbol{\eta} := (\eta_1, \dots, \eta_M)^T \in \mathbb{R}^M$ such that

$$\begin{cases} \sum_{i=1}^N \xi_i \left(a_h^\Omega(\varphi_i,\varphi_j) + m_h^\Omega(\varphi_i,\varphi_j)\right) + \sum_{k=1}^M \left(\alpha\xi_k m_h^\Gamma(\varphi_k,\varphi_l) - \beta\eta_k m_h^\Gamma(\psi_k,\varphi_l)\right) = \sum_{i=1}^N f(\boldsymbol{x}_i) m_h^\Omega(\varphi_i,\varphi_j); \\ \sum_{k=1}^M (\eta_k a_h^\Gamma(\psi_k,\psi_l) - \alpha\xi_k m_h^\Gamma(\varphi_k,\psi_l) + (\beta+1)\eta_k m_h^\Gamma(\psi_k,\psi_l)) = \sum_{k=1}^M g(\boldsymbol{x}_k) m_h^\Gamma(\psi_k,\psi_l), \end{cases} \tag{56}$$

for all $j = 1, \dots, N$ and $l = 1, \dots, M$. We define the matrices $A_\Omega = (a_{i,j}^\Omega) \in \mathbb{R}^{N\times N}$, $M_\Omega = (m_{i,j}^\Omega) \in \mathbb{R}^{N\times N}$, $A_\Gamma = (a_{k,l}^\Gamma) \in \mathbb{R}^{M\times M}$ and $M_\Gamma = (m_{k,l}^\Gamma) \in \mathbb{R}^{M\times M}$ as follows:

$$a_{i,j}^\Omega := a_h^\Omega(\varphi_i,\varphi_j), \quad \text{and} \quad m_{i,j}^\Omega := m_h^\Omega(\varphi_i,\varphi_j), \qquad i,j = 1, \dots, N; \tag{57}$$

$$a_{k,l}^\Gamma := a_h^\Gamma(\psi_k,\psi_l), \quad \text{and} \quad m_{k,l}^\Gamma := m_h^\Gamma(\psi_k,\psi_l), \qquad k,l = 1, \dots, M. \tag{58}$$

By using (34) and defining $\boldsymbol{f} := (f(\boldsymbol{x}_1), \dots, f(\boldsymbol{x}_N))^T \in \mathbb{R}^N$ and $\boldsymbol{g} := (g(\boldsymbol{x}_1), \dots, g(\boldsymbol{x}_M))^T \in \mathbb{R}^M$ we can rewrite the discrete formulation (56) as a block $(N+M)\times(N+M)$ linear algebraic system:

$$\begin{cases} A_\Omega\boldsymbol{\xi} + M_\Omega\boldsymbol{\xi} + \alpha R M_\Gamma R^T\boldsymbol{\xi} - \beta R M_\Gamma\boldsymbol{\eta} = M_\Omega\boldsymbol{f}; \\ A_\Gamma\boldsymbol{\eta} - \alpha M_\Gamma R^T\boldsymbol{\xi} + (\beta+1) M_\Gamma\boldsymbol{\eta} = M_\Gamma\boldsymbol{g}, \end{cases} \tag{59}$$

where R is the reduction matrix defined in Section 3.1. In compact form, the linear system (59) reads

$$\begin{bmatrix} A_\Omega + M_\Omega + \alpha R M_\Gamma R^T & -\beta R M_\Gamma \\ -\alpha M_\Gamma R^T & A_\Gamma + (\beta+1) M_\Gamma \end{bmatrix} \begin{bmatrix} \boldsymbol{\xi} \\ \boldsymbol{\eta} \end{bmatrix} = \begin{bmatrix} M_\Omega\boldsymbol{f} \\ M_\Gamma\boldsymbol{g} \end{bmatrix}. \tag{60}$$

It is possible to show that the coefficient matrix of (60) is sparse and unstructured.

We conclude this section by outlining the challenges involved in extending the BSVEM to the higher order case.

> *Remark* 2 (Extension of BSVEM to higher order)**.** Lemma 1 implies that curved polyhedral meshes are necessary to achieve higher order spatial convergence. The main challenge in devising a higher order BS-VEM resides in the construction of discrete function spaces $\mathbb{V}_\Omega$ and $\mathbb{V}_\Gamma$ on curved meshes, such that the discrete bilinear forms (49) and (50) are computable. For the bulk space $\mathbb{V}_\Omega$, the problem was addressed in special cases: (i) in 2D where Γ is a curve [14] and (ii) in 3D for a Darcy problem in mixed form [29]. To the best of the authors' knowledge, the problem for 3D differential operators in non-mixed form

is still an open problem. For the surface space $\mathbb{V}_\Gamma$, a parametric VEM relying on explicitly known local charts was proposed in [5]. An additional challenge is that the coupling condition given by the third equation in (1) constrains the surface space $\mathbb{V}_\Gamma$ to be the trace of the bulk space $\mathbb{V}_\Omega$, so the two spaces cannot be constructed independently from each other. A high order BSVEM that simultaneously addresses these challenges is part of our current investigations.

5 | CONVERGENCE ANALYSIS

To derive error estimates for the discrete solution we need a bulk-surface Ritz projection tailored for the variational problem (3).

Definition 5 (Bulk-Surface Ritz projection)**.** The bulk-surface Ritz projection of a pair $(u, v) \in H^1(\Gamma) \times H^1(\Omega)$ is the unique pair $(\mathcal{R}u, \mathcal{R}v) \in \mathbb{V}_\Omega \times \mathbb{V}_\Gamma$ such that

$$b_h((\mathcal{R}u, \mathcal{R}v); (\varphi, \psi)) = b((u, v); (\varphi^\ell, \psi^\ell)), \qquad \forall (\varphi, \psi) \in \mathbb{V}_\Omega \times \mathbb{V}_\Gamma. \tag{61}$$

The bulk-surface Ritz projection is well-defined since b_h is coercive.

Theorem 2 ($H^1(\Omega) \times H^1(\Gamma)$ a priori error bound for the bulk-surface Ritz projection)**.** *For any $(u, v) \in H^{2+3/4}(\Omega) \times H^2(\Gamma)$ it holds that*

$$\|(u, v) - (\mathcal{R}u, \mathcal{R}v)^\ell\|_{H^1(\Omega)\times H^1(\Gamma)} \leq Ch\|(u, v)\|_{H^{2+3/4}(\Omega)\times H^2(\Gamma)}, \tag{62}$$

where the additional index $3/4$ appears only in the simultaneous presence of curved boundaries and non-tetrahedral exterior elements.

Proof. We set $e_h = (e_h^\Omega, e_h^\Gamma) := (\mathcal{R}u - u^{-\ell}, \mathcal{R}v - v^{-\ell})$. From (46)–(48), and (61) we have

$$\begin{aligned}\alpha_* \min(\alpha, \beta)\|e_h\|_{H^1(\Omega)\times H^1(\Gamma)} \leq b_h(e_h, e_h) = \alpha \left(\underbrace{a_h^\Omega(e_h^\Omega, e_h^\Omega)}_{T_1} + \underbrace{m_h^\Omega(e_h^\Omega, e_h^\Omega)}_{T_2} \right) \\ + \beta \left(\underbrace{a_h^\Gamma(e_h^\Gamma, e_h^\Gamma)}_{T_3} + \underbrace{m_h^\Gamma(e_h^\Gamma, e_h^\Gamma)}_{T_4} \right) + \underbrace{m_h^\Gamma(\alpha e_h^\Omega - \beta e_h^\Gamma, \alpha e_h^\Omega - \beta e_h^\Gamma)}_{T_5}.\end{aligned} \tag{63}$$

We estimate T_1 using (16), (21), (30), (46), (61) and the continuity of a_h^Ω:

$$\begin{aligned}T_1 &= a_h^\Omega(\mathcal{R}u, e_h) - a_h^\Omega(u^{-\ell}, e_h) = \int_\Omega \nabla u \cdot \nabla e_h^\ell + a_h^\Omega(\widetilde{u} - u^{-\ell}, e_h) + a_h^\Omega(\widetilde{u}_\pi - \widetilde{u}, e_h) - a_h^\Omega(\widetilde{u}_\pi, e_h) \\ &= \int_\Omega \nabla u \cdot \nabla e_h^\ell - \int_{\Omega_h} \nabla \widetilde{u}_\pi \cdot \nabla e_h + a_h^\Omega(\widetilde{u} - u^{-\ell}, e_h) + a_h^\Omega(\widetilde{u}_\pi - \widetilde{u}, e_h) \\ &= \int_\Omega \nabla u \cdot \nabla e_h^\ell - \int_{\Omega_h} \nabla u^{-\ell} \cdot \nabla e_h + \int_{\Omega_h} \nabla(u^{-\ell} - \widetilde{u}) \cdot \nabla e_h + \int_{\Omega_h} \nabla(\widetilde{u} - \widetilde{u}_\pi) \cdot \nabla e_h \\ &\quad + a_h^\Omega(\widetilde{u} - u^{-\ell}, e_h) + a_h^\Omega(\widetilde{u}_\pi - \widetilde{u}, e_h) \\ &\leq C \left(h\|u\|_{H^2(\Omega)} + h^{\frac{3}{2}}\|u\|_{H^2(\Omega)} + Ch\|u\|_{H^{2+3/4}(\Omega)} \right) |e_h|_{H^1(\Omega_h)}.\end{aligned} \tag{64}$$

We estimate T_2 in the same way by using (17), (21), (30), (46) and the continuity of m_h^Ω:

$$T_2 \leq Ch^2 \left(\|u\|_{H^2(\Omega)} + \|u\|_{H^{2+1/4}(\Omega)} \right) \|e_h\|_{L^2(\Omega_h)}. \tag{65}$$

We estimate T_3 by reasoning as for T_1, but this time there is no need for the Sobolev extension because, as opposed to the $H^2(\Omega)$ norm, the $H^2(\Gamma)$ norm is preserved under lifting thanks to (15). This implies that $v^{-\ell}$ is H^2 on each face of Γ_h and thus fulfils the optimal error estimate for the projection (31). Hence, by using (18), (31), and (45), the estimate for T_3 reads as follows:

$$\begin{aligned}
T_3 &= a_h^\Gamma(\mathcal{R}v, e_h^\Gamma) - a_h^\Gamma(v^{-\ell}, e_h^\Gamma) = \int_\Gamma \nabla_\Gamma v \cdot \nabla_\Gamma e_h^{\Gamma,\ell} + a_h^\Gamma(v_\pi^{-\ell} - v^{-\ell}, e_h) - a_h^\Gamma(v_\pi^{-\ell}, e_h^\Gamma) \\
&= \int_\Gamma \nabla_\Gamma v \cdot \nabla_\Gamma e_h^{\Gamma,\ell} - \int_{\Gamma_h} \nabla_{\Gamma_h} v_\pi^{-\ell} \cdot \nabla_{\Gamma_h} e_h^\Gamma + a_h^\Gamma(v_\pi^{-\ell} - v^{-\ell}, e_h^\Gamma) \\
&= \int_\Gamma \nabla_\Gamma v \cdot \nabla_\Gamma e_h^{\Gamma,\ell} - \int_{\Gamma_h} \nabla_{\Gamma_h} v^{-\ell} \cdot \nabla_{\Gamma_h} e_h^\Gamma + \int_{\Gamma_h} \nabla_{\Gamma_h}(v^{-\ell} - v_\pi^{-\ell}) \cdot \nabla_{\Gamma_h} e_h^\Gamma + a_h^\Gamma(v_\pi^{-\ell} - v^{-\ell}, e_h^\Gamma) \\
&\leq Ch \|v\|_{H^2(\Gamma)} |e_h|_{H^1(\Gamma_h)}.
\end{aligned} \tag{66}$$

We estimate T_4 in the same way as T_3, by using (19) instead of (18) and choosing $s = 1$ instead of $s = 2$ in (30):

$$T_4 \leq Ch \|v\|_{H^1(\Gamma)} \|e_h\|_{L^2(\Gamma_h)}. \tag{67}$$

We estimate T_5 exactly as T_4 and then we apply the inverse trace inequality (A5) in Appendix A:

$$\begin{aligned}
T_5 &\leq Ch \left(\|v\|_{H^1(\Gamma)} + \|\mathrm{Tr} u\|_{H^1(\Gamma)} \right) \left(\|e_h^\Gamma\|_{L^2(\Gamma_h)} + \|\mathrm{Tr} e_h^\Omega\|_{L^2(\Gamma_h)} \right) \\
&\leq Ch \left(\|v\|_{H^1(\Gamma)} + \|u\|_{H^2(\Gamma)} \right) \left(\|e_h^\Gamma\|_{L^2(\Gamma_h)} + \|e_h^\Omega\|_{H^1(\Gamma_h)} \right).
\end{aligned} \tag{68}$$

By substituting (64)–(68) into (63) and applying a Young inequality argument, we get the desired estimate (62). In (64) and (65) notice that, in the absence of curvature or non-tetrahedral exterior elements, $u_{|E}^{-\ell} \in H^2(E)$ for all elements $E \in \mathcal{E}_h$, see Remark 1. Then the Sobolev extension $\widetilde{u}$ is not needed and the terms in $H^{2+3/4}(\Omega)$ and $H^{2+1/4}(\Omega)$ do not appear. This completes the proof. ∎

Theorem 3 ($L^2(\Omega) \times L^2(\Gamma)$ error bound for the bulk-surface Ritz projection)**.** *Let Ω have a C^3 boundary. Then, for any $(u, v) \in H^{2+3/4}(\Omega) \times H^2(\Gamma)$ and for h sufficiently small, it holds that*

$$\|(u, v) - (\mathcal{R}u, \mathcal{R}v)^\ell\|_{L^2(\Omega)\times L^2(\Gamma)} \leq Ch^2 \|(u, v)\|_{H^{2+3/4}(\Omega)\times H^2(\Gamma)}, \tag{69}$$

with $C > 0$ depending on Ω, γ_1 and γ_2. In (69), the additional exponent $3/4$ arises only in the simultaneous presence of curved boundaries and non-tetrahedral exterior elements.

Proof. We will use an adapted Aubin-Nitsche duality method. Consider the dual problem: find $(\eta, \theta) \in H^1(\Omega) \times H^1(\Gamma)$ such that

$$b((\eta, \theta); (\varphi, \psi)) = \int_\Omega (u - (\mathcal{R}u)^\ell)\varphi + \int_\Gamma (v - (\mathcal{R}v)^\ell)\psi, \tag{70}$$

for all $(\varphi, \psi) \in H^1(\Omega) \times H^1(\Gamma)$. Since $u - (\mathcal{R}u)^\ell \in H^1(\Omega)$, thanks to (5), the variational problem (70) has a unique solution $(\eta, \theta) \in H^3(\Omega) \times H^2(\Gamma)$ that fulfils

$$\|(\eta,\theta)\|_{H^3(\Omega)\times H^2(\Gamma)} \le C\|(u,v)-(\mathcal{R}u,\mathcal{R}v)^\ell)\|_{H^1(\Omega)\times H^1(\Gamma)}. \tag{71}$$

By combining (62) and (71) we have that

$$\|(\eta,\theta)\|_{H^3(\Omega)\times H^2(\Gamma)} \le Ch\|(u,v)\|_{H^2(\Omega)\times H^2(\Gamma)} + Ch\|u\|_{H^{2+3/4}(\Omega)}. \tag{72}$$

We can choose $(\varphi,\psi)=(e_h^\Omega,e_h^\Gamma)=(u,v)-(\mathcal{R}u,\mathcal{R}v)^\ell$ in (70) and we get

$$\|(u,v)-(\mathcal{R}u,\mathcal{R}v)^\ell\|^2_{L^2(\Omega)\times L^2(\Gamma)} = \int_\Omega \varphi^2 + \int_\Gamma \psi^2 = b((\eta,\theta);(u-\mathcal{R}u^\ell, v-\mathcal{R}v^\ell)). \tag{73}$$

The right hand side of (73) can be split into five terms, say $\overline{T}_1,\ \dots\ ,\overline{T}_5$ as in (63). We explicitly show the estimation of the first of such terms—the most involved. The treatment of the other terms is similar. By using (16) and (61) we have

$$\begin{aligned}
\overline{T}_1 &:= a_h^\Omega(\eta,e_h^\Omega) = \int_\Omega \nabla\eta\cdot\nabla\left(u-(\mathcal{R}u)^\ell\right)\\
&= \int_\Omega \nabla\left(u-(\mathcal{R}u)^\ell\right)\cdot\nabla\left(\eta-I_\Omega(\widetilde{\eta})^\ell\right) - \int_\Omega \nabla(\mathcal{R}u)^\ell\cdot\nabla I_\Omega(\widetilde{\eta})^\ell + a_h(\mathcal{R}u,I_\Omega(\widetilde{\eta}))\\
&\le |u-(\mathcal{R}u)^\ell|_{H^1(\Omega)}|\eta-I_\Omega(\widetilde{\eta})^\ell|_{H^1(\Omega)} - \int_\Omega \nabla(\mathcal{R}u)^\ell\cdot\nabla I_\Omega(\widetilde{\eta})^\ell + a_h(\mathcal{R}u,I_\Omega(\widetilde{\eta}))\\
&\le |u-(\mathcal{R}u)^\ell|_{H^1(\Omega)}|\eta-I_\Omega(\widetilde{\eta})^\ell|_{H^1(\Omega)} + Ch|(\mathcal{R}u)^\ell|_{H^1(\Omega_B^\ell)}|I_\Omega(\widetilde{\eta})|_{H^1(\Omega_B^\ell)}\\
&\quad - \int_{\Omega_h}\nabla\mathcal{R}u\cdot\nabla I_\Omega(\widetilde{\eta}) + a_h(\mathcal{R}u,I_\Omega(\widetilde{\eta}))\\
&\le C\left(|u-(\mathcal{R}u)^\ell|_{H^1(\Omega)} + h^{\frac12}|u|_{H^1(\Omega_B^\ell)}\right)\left(|\eta-I_\Omega(\widetilde{\eta})^\ell|_{H^1(\Omega)} + h^{\frac12}|\eta|_{H^1(\Omega_B^\ell)}\right)\\
&\quad - \int_{\Omega_h}\nabla\mathcal{R}u\cdot\nabla I_\Omega(\widetilde{\eta}) + a_h^\Omega(\mathcal{R}u,I_\Omega(\widetilde{\eta})),
\end{aligned} \tag{74}$$

where we have used $h<h_0$ in the last inequality. We are left to estimate the right-hand-side of (74) piecewise. First, from (62) and (A3) in Appendix A we have that

$$|u-(\mathcal{R}u)^\ell|_{H^1(\Omega)} + h^{\frac12}|u|_{H^1(\Omega_B^\ell)} \le Ch\|(u,v)\|_{H^2(\Omega)\times H^2(\Gamma)} + Ch\|u\|_{H^{2+3/4}(\Omega)}. \tag{75}$$

Moreover, from (21), (51), (71), (72), and (A3), (A6) in Appendix A, we have that

$$\begin{aligned}
|\eta-I_\Gamma(\widetilde{\eta})^\ell|_{H^1(\Omega)} + h^{\frac12}|\eta|_{H^1(\Omega_B^\ell)} &\le C|\eta^{-\ell}-I_\Gamma(\widetilde{\eta})|_{H^1(\Omega_h)} + Ch\|\eta\|_{H^2(\Omega)}\\
&\le C|\eta^{-\ell}-\widetilde{\eta}|_{H^1(\Omega_h)} + C|\widetilde{\eta}-I_\Gamma(\widetilde{\eta})|_{H^1(\Omega_h)} + Ch\|\eta\|_{H^2(\Omega)}\\
&\le Ch^2\|\eta\|_{H^3(\Omega)} + Ch\|\widetilde{\eta}\|_{H^2(\Omega_h)} + Ch\|\eta\|_{H^2(\Omega)} \le Ch\|\eta\|_{H^2(\Omega)} + Ch^2\|\eta\|_{H^3(\Omega)}\\
&\le Ch\|u-(\mathcal{R}u)^\ell\|_{L^2(\Omega)} + Ch^3\|(u,v)\|_{H^2(\Omega)\times H^2(\Gamma)} + Ch^3\|u\|_{H^{2+3/4}(\Omega)}.
\end{aligned} \tag{76}$$

Finally, we estimate the last two terms in (74) by adapting the approach used in [60, Lemma 3.1]: from (21), (30), (46), (51), and (71) we have

$$\begin{aligned}
a_h^\Omega(\mathcal{R}u,I_\Omega(\widetilde{\eta})) - \int_{\Omega_h}\nabla\mathcal{R}u\cdot\nabla I_\Omega(\widetilde{\eta}) &= \int_{\Omega_h}\nabla(\mathcal{R}u-\widetilde{u}_\pi)\cdot\nabla(I_\Omega(\widetilde{\eta})-\widetilde{\eta}_\pi) - a_h^\Omega(\mathcal{R}u-\widetilde{u}_\pi,I_\Omega(\widetilde{\eta})-\widetilde{\eta}_\pi)\\
&\le |\mathcal{R}u-\widetilde{u}_\pi|_{1,\Omega,h}|I_\Gamma(\widetilde{\eta})-\widetilde{\eta}_\pi|_{1,\Omega,h} \le Ch\|(u,v)\|_{H^{2+3/4}(\Omega)\times H^2(\Gamma)}Ch\|\eta\|_{H^2(\Omega)}\\
&= Ch^2\|(u,v)\|_{H^{2+3/4}(\Omega)\times H^2(\Gamma)}\|u-(\mathcal{R}u)^\ell\|_{L^2(\Omega)}.
\end{aligned} \tag{77}$$

By combining (74)–(77) we get

$$\overline{T}_1 \le Ch^2\|(u,v)\|_{H^{2+3/4}(\Omega)\times H^2(\Gamma)}\|e_h^\Omega\|_{L^2(\Omega)} + Ch^4\|(u,v)\|^2_{H^{2+3/4}(\Omega)\times H^2(\Gamma)}. \tag{78}$$

By estimating all remaining terms $\overline{T}_2 \dots, \overline{T}_5$ as $\overline{T}_1$ in (78) and substituting into (73) we get

$$\|(e_h^\Omega, e_h^\Gamma)\|^2_{L^2(\Omega)\times L^2(\Gamma)} \leq Ch^2 \|(u,v)\|_{H^{2+3/4}(\Omega)\times H^2(\Gamma)} \|(e_h^\Omega, e_h^\Gamma)\|_{L^2(\Omega)\times L^2(\Gamma)} + Ch^4 \|(u,v)\|^2_{H^{2+3/4}(\Omega)\times H^2(\Gamma)},$$

where the additional index $3/4$ appears only in the simultaneous presence of curved boundaries and non-tetrahedral exterior elements, which proves (69). ∎

Theorem 4 ($L^2(\Omega)\times L^2(\Gamma)$ and $H^1(\Omega)\times H^1(\Gamma)$ error bounds for the BSVEM)**.** *Let Ω have a C^3 boundary. Then, if $(f,g) \in H^{2+1/4}(\Omega)\times H^2(\Gamma)$, the numerical solution (U,V) fulfils*

$$\|(u,v) - (U,V)^\ell\|_{L^2(\Omega)\times L^2(\Gamma)} + h|(u,v) - (U,V)^\ell|_{H^1(\Omega)\times H^1(\Gamma)} \leq Ch^2 \|(f,g)\|_{H^{2+1/4}(\Omega)\times H^2(\Gamma)}, \quad (79)$$

with $C > 0$ depending on Ω, γ_1 and γ_2. In (79), the additional index $1/4$ arises only in the simultaneous presence of curved boundaries and non-tetrahedral exterior elements.

Proof. The proof relies on a standard error equation technique. The difference $(u,v) - (\mathcal{R}u, \mathcal{R}v)^\ell$ is estimated in both $L^2(\Omega)\times L^2(\Gamma)$ norm and $H^1(\Omega)\times H^1(\Gamma)$ seminorm via (62) and (69), respectively. It remains to estimate the term $(\mathcal{R}u, \mathcal{R}v)^\ell - (U,V)^\ell$. To this end we use the following error equation obtained by subtracting the discrete problem (53) from the weak continuous problem (3) and using (61):

$$b_h((\mathcal{R}u - U, \mathcal{R}v - V); (\varphi, \psi)) = \int_\Omega f\varphi^\ell - m_h^\Omega(I_\Omega(f), \varphi) + \int_\Gamma g\psi^\ell - m_h^\Gamma(I_\Gamma(g), \psi). \quad (80)$$

By choosing $\varphi = \mathcal{R}u - U$ and $\psi = \mathcal{R}v - V$, we estimate the left hand side of (80) using (45) and (46), and the right hand side via (17), (19), (20), (51), and (52). It follows that

$$\|(\mathcal{R}u, \mathcal{R}v)^\ell - (U,V)^\ell\|_{H^1(\Omega)\times H^1(\Gamma)} \leq Ch^2 \|(f,g)\|_{H^{2+1/4}(\Omega)\times H^2(\Gamma)}, \quad (81)$$

that is, the term $\|(\mathcal{R}u, \mathcal{R}v)^\ell - (U,V)^\ell\|_{H^1(\Omega)\times H^1(\Gamma)}$ superconvergences quadratically in $H^1(\Omega)\times H^1(\Gamma)$ norm, as usual in the Ritz-Galerkin method. The claim follows. ∎

Remark 3 (Optimal convergence for bulk-only PDEs)**.** By considering the limit case $\beta = 0$ in the model problem (1), the bulk equation becomes completely decoupled from the surface equation. Specifically, the first equation in (1) becomes a linear elliptic equation in the 3D domain Ω, endowed with non-zero Neumann boundary conditions. Correspondingly, the BSVEM reduces to the known lowest-order VEM for elliptic problems in 3D (see [7]). Then, by setting $\beta = 0$ throughout the present section devoted to convergence analysis, we obtain that the lowest-order VEM for 3D elliptic bulk problems retains optimal convergence in the presence of curved boundaries and non-zero boundary conditions. As mentioned in the Introduction, this result was not fully addressed in the literature, in this work we provide a rigorous justification. It must be noted that previous works addressed the issue through the introduction of curved boundaries (see [14, 29]) or the introduction of algebraic corrections in the method that account for surface curvature (see [17]). Here, we show for the first time that the plain 3D VEM of lowest order possesses optimal convergence even in the presence of curved boundaries.

6 | BENEFITS OF POLYHEDRAL MESHES FOR BSPDES

If a domain $\Omega \subset \mathbb{R}^3$ has a C^1 boundary Γ, we can construct a polyhedral mesh designed for fast matrix assembly, by proceeding as follows. Enclose the bulk Ω in a cube Q. We discretize Q with a Cartesian grid made up of cubic mesh elements and assume that at least one of such cubes is fully contained in Ω (see Figure 3a). Then we discard the elements that are fully outside Ω, possibly touching Γ (see Figure 3b), thereby producing an incomplete cubic mesh. Finally, we cut the cubic elements that intersect Γ, thus producing a discrete narrow band Ω_B of irregular polyhedral elements (highlighted in red in Figure 3c). The resulting mesh Ω_h has the important property that it is made up of equal cubic elements, except for the exterior elements, as we can see in Figure 3c.

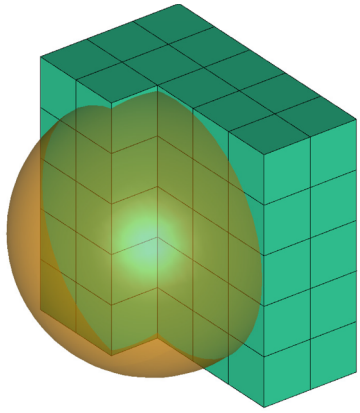

(a) Step 1. The bulk Ω, enclosed by the orange boundary Γ, is bounded by the green cube Q, which is subdivided with a Cartesian grid.

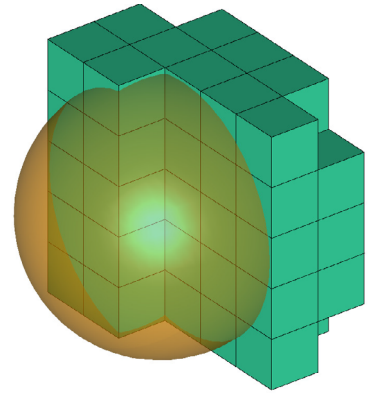

(b) Step 2. The cubic elements that are fully outside Ω are discarded.

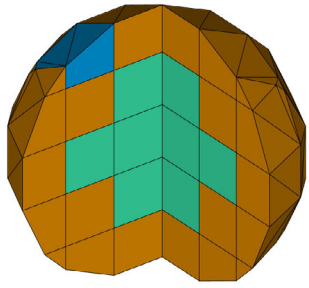

(c) Step 3. The cubic elements that intersect Γ are cut, thereby producing the orange band of polyhedral elements. One of the cut elements is highlighted in blue.

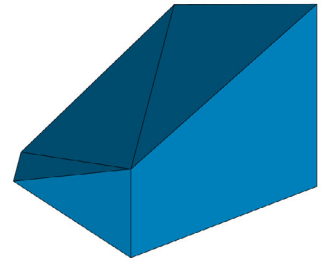

(d) The blue polyhedral element in Fig. 3(c) generated through the cutting process.

FIGURE 3 Generation of a polyhedral bulk-surface mesh that allows for optimized matrix assembly.

This property allows for fast matrix assembly. In fact if h is the meshsize of Ω_h, then the number on non-cubic elements of Ω_h is only $\mathcal{O}(h^{-2})$ out of $\mathcal{O}(h^{-3})$ overall elements, see [35] for a discussion of the 2D case. This implies that, when assembling the mass- and stiffness- matrices M_Ω and A_Ω defined in (57), only $\mathcal{O}(h^{-2})$ element-wise local matrices must be actually computed, since the local matrices for a cubic element can be computed in closed form, see [9]. For ease of presentation, the above mesh generation strategy is illustrated for a spherical domain in Figure 3, but applies to all shapes defined as level sets of Lipschitz functions. For instance, consider the level function

$$\lambda(x,y,z) := \left(9(x^2+y^2+z^2)+\frac{261}{100}\right)^2 - 4\left(6x-\frac{\sqrt{39}}{100}\right)^2 - \frac{3249}{25}y^2, \qquad (x,y,z)\in\mathbb{R}^3. \tag{82}$$

This level function gives rise to the *Dupin ring cyclide* $\Gamma = \{(x,y,z)\in\mathbb{R}^3 | \lambda(x,y,z) = 0\}$ considered in [39, 42], which encloses the *bulk cyclide* $\Omega := \{(x,y,z)\in\mathbb{R}^3 | \lambda(x,y,z) \le 0\}$. In Figure 4, we show the bulk cyclide Ω and a corresponding mesh generated with the above algorithm.

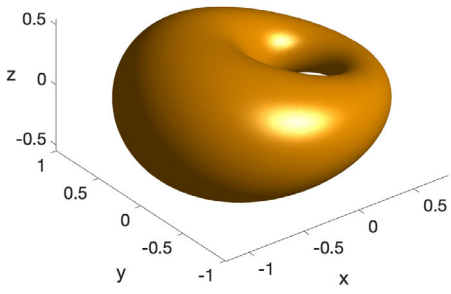

(a) Dupin ring cyclide defined in (82)

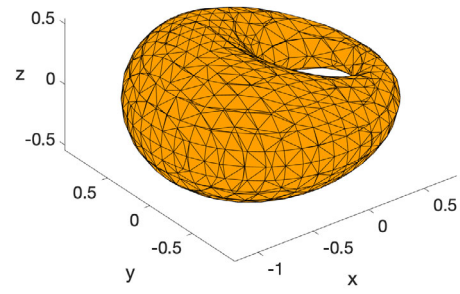

(b) Mesh with N = 11880 nodes and meshsize h = 0.1039.

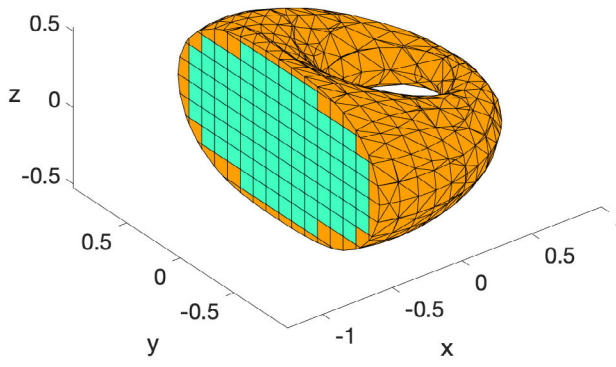

(c) Cross-section of the mesh, which shows the interior being composed of cubes.

FIGURE 4 Dupin ring cyclide defined in (82) and a mesh for such domain, generated with the algorithm described in Section 6. The mesh has N = 11,880 nodes and meshsize h = 0.1039.

TABLE 1 Elliptic BSPDE (83) on the unit sphere Ω in 3D.

i	N	M	h	$L^2(\Omega)\times L^2(\Gamma)$ rel. err.	L^2 EOC	$H^1(\Omega)\times H^1(\Gamma)$ rel. err.	H^1 EOC	Time (s)
1	152	96	0.7205	1.2114e−01	-	1.6937e−01	-	0.002554
2	875	414	0.3602	1.8409e−02	2.7182	4.6517e−02	1.8643	0.016998
3	5501	1758	0.1801	4.9571e−03	1.8928	2.3725e−02	0.9714	0.194121
4	36,677	6966	0.0901	1.2578e−03	1.9786	1.0147e−02	1.2254	5.880451

Note: The BSVEM shows optimal convergence, that is, quadratic in $L^2(\Omega)\times L^2(\Gamma)$ and linear in $H^1(\Omega)\times H^1(\Gamma)$. The computational times are shown.
Abbreviation: EOC, experimental order of convergence.

Matrix assembly optimization can also be achieved with different methods, such as cut FEM [22] or trace FEM [44]. In the present work, however, the numerical method does not require a level set representation of the surface Γ. Such a level set representation is needed only upon mesh generation, if the mesh is generated as described in this section. Moreover, the proposed approach is an adaptation to 3D of the mesh generation algorithm proposed in [35] for the 2D case.

7 | NUMERICAL EXAMPLES

We present two numerical examples to (i) showcase the construction of polyhedral meshes according to the procedure explained in Section 6 and (ii) confirm the optimal convergence of the BSVEM according to Theorem 4.

7.1 | Example 1: Unit sphere

We numerically solve the following elliptic bulk-surface problem on the unit sphere Ω in 3D:

$$\begin{cases} -\Delta u + u = xyz - xy & \text{in } \Omega \\ -\Delta_\Gamma v + v + \nabla u \cdot \boldsymbol{\nu} = 29xyz - \frac{25}{2}xy & \text{on } \partial\Omega \\ \nabla u \cdot \boldsymbol{\nu} = -u + 2v & \text{on } \partial\Omega, \end{cases} \tag{83}$$

whose exact solution is given by $u(x,y,z) = xyz - xy$, for $(x,y,z) \in \Omega$ and $v(x,y,z) = 2xyz - \frac{3}{2}xy$, for $(x,y,z) \in \partial\Omega$. We consider a sequence of four cubic meshes $i = 1, \dots, 4$. The ith mesh is obtained by subdividing each dimension into $5i$ intervals, thereby producing a cubic bounding mesh. From the cubic mesh we obtain a bulk-surface mesh of the sphere as described in Section 6. The coarsest of meshes is shown in Figure 3c. On each mesh we solve the discrete problem (60), we compute the relative error in $L^2(\Omega)\times L^2(\Gamma)$ and $H^1(\Omega)\times H^1(\Gamma)$ norms and the respective convergence rates by the direct solver `mldivide` of MATLAB R2019a on a MacBook Pro 2019 with 2,3 GHz 8-Core Intel Core i9 CPU. As shown in Table 1, the convergence is optimal, that is, quadratic in $L^2(\Omega)\times L^2(\Gamma)$ norm and linear in $H^1(\Omega)\times H^1(\Gamma)$ norm, according to Theorem 4. The numerical solution (U,V) obtained on the finest mesh is plotted in Figure 5, where the bulk component U and the surface component V are shown in separate plots, both cut to show the inside.

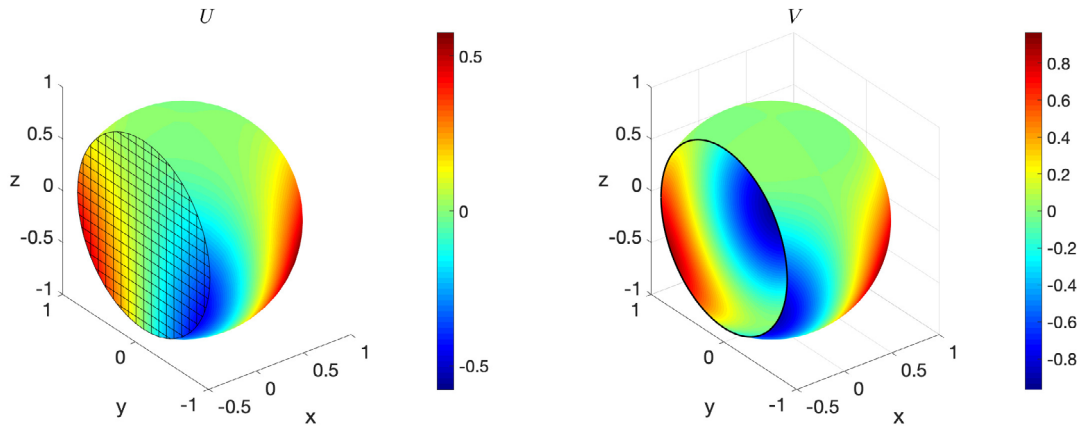

FIGURE 5 Elliptic bulk-surface problem (83) on the unit sphere Ω in 3D: Numerical solution obtained on the finest mesh for $i = 4$ with $N = 40{,}381$ nodes and meshsize $h = 0.0901$. Components U (left) and V (right) of the numerical solution.

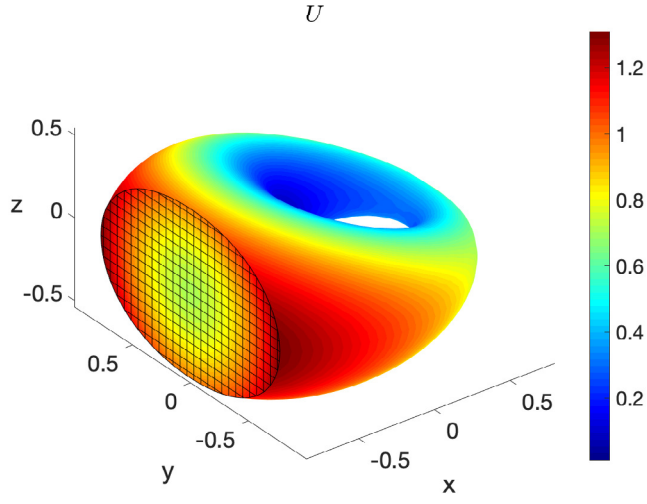

FIGURE 6 Bulk component u of the numerical solution of model (84) obtained on the polyhedral mesh shown in Figure 4b,c with $N = 11{,}880$ nodes and meshsize $h = 0.1039$. The figure is cut to show the interior of the bulk.

7.2 | Example 2: Dupin ring cyclide

Having ascertained the optimal convergence of the method in the previous example, we now explore a more complex geometry given by the Dupin ring cyclide Ω defined in (82) and shown in Figure 4a. On such a geometry, we consider the model problem

$$\begin{cases} -\Delta u + u = x^2 + y^2 + z^2 - 6, & \text{in } \Omega; \\ -\Delta_\Gamma v + u + v = x^2 + y^2 + z^2 + 1, & \text{on } \Gamma; \\ \nabla u \cdot \boldsymbol{\nu} = \rho(x, y, z) - v + 1, & \text{on } \Gamma, \end{cases} \tag{84}$$

where

$$\rho(x, y, z) := \frac{\nabla \lambda(x, y, z) \cdot (2x, 2y, 2z)}{\|\nabla \lambda(x, y, z)\|}, \qquad (x, y, z) \in \Gamma, \tag{85}$$

with $\lambda(x, y, z)$ being the level function defined in (82) and the exact solution is given by[1]

$$u(x, y, z) = x^2 + y^2 + z^2, \quad (x, y, z) \in \Omega, \qquad \text{and} \qquad v(x, y, z) = 1, \quad (x, y, z) \in \Gamma. \tag{86}$$

We solve the model (84) on the mesh shown in Figure 4b,c. The mesh has $N = 11{,}880$ nodes and meshsize $h = 0.1039$. The relative errors are: 1.7962e−03 in $L^2(\Omega) \times L^2(\Gamma)$ norm and 4.5671e−03 in $H^1(\Omega) \times H^1(\Gamma)$ norm, which further confirms the accuracy of the method. Since the surface component $v(x, y, z)$ of the exact solution is constant, we plot only the bulk component $u(x, y, z)$ of the numerical solution in Figure 6.

8 | CONCLUSIONS

We have introduced the BSVEM for the numerical approximation of elliptic coupled bulk-surface PDE problems on smooth domains. The proposed method combines a 3D VEM for the bulk equations [10] with a SVEM for the surface equations [40] and encompasses, in the special case of simplicial bulk-surface meshes, the BSFEM for bulk-surface RDSs (see e.g., [51]).

We have introduced polyhedral bulk-surface meshes in 3D and, under minimal mesh regularity assumptions, we have estimated the geometric error arising from domain approximation. The lack of smoothness in the mapping between the discrete and exact geometries requires the lifting operator to be replaced, in some parts of the analysis, by the Sobolev extension operator.

The main theoretical result is optimal second-order convergence of the proposed method, provided the exact solution is $H^{2+3/4}$ in the bulk and H^2 on the surface. A relevant by-product is that the lowest order bulk-VEM [7] retains optimal convergence even in the simultaneous presence of curved boundaries and non-zero boundary conditions, a result that was not fully addressed in the literature to the best of our knowledge. The convergence is illustrated with two numerical examples on the unit sphere and on the Dupin ring cyclide, respectively.

We have shown that suitable polyhedral meshes reduce the computational time of mesh generation and matrix assembly from $\mathcal{O}(h^{-3})$ to $\mathcal{O}(h^{-2})$, where h is the meshsize. This is particularly useful when matrix assembly takes a significant portion of the computational time, that is, for (i) time-independent problems and (ii) time-dependent problems on evolving domains, where the matrices must be computed at each timestep.

In different geometric settings and for different PDE problems, it is known that polyhedral meshes also allow for simple and efficient adaptive refinement or mesh pasting strategies that would be impossible with tetrahedral meshes, see for instance [23]. For the BSVEM, these aspects will be addressed in future studies.

Another subject of our current investigation is the formulation of a high-order BSVEM. As pointed out throughout the work, this goal entails (i) the usage of curved polyhedral meshes and (ii) the construction of computable discrete function spaces on curved polygons and polyhedra. Finally, we will consider the extension of the BSVEM to the case of evolving bulk-surface geometries.

ACKNOWLEDGMENTS

The work of MF was funded by Regione Puglia (Italy) through the research programme REFIN-Research for Innovation (protocol code 901D2CAA, project number UNISAL026) and by

[1]The surface component $v(x, y, z)$ of the exact solution is chosen constant because the Laplace–Beltrami Δ_Γ of a non-constant function is extremely cumbersome to compute. This issue can be circumvented on special geometries, like the sphere of the previous numerical example, where some eigenfunctions of Δ_Γ are known in closed form.

the Italian National Group of Scientific Computing (INdAM-GNCS) through the research project "Metodi numerici innovativi per lo studio delle batterie" (project CUP E55F22000270001). This work (AM) was partly supported by the Global Challenges Research Fund through the Engineering and Physical Sciences Research Council grant number EP/T00410X/1: UK-Africa Postgraduate Advanced Study Institute in Mathematical Sciences, the Health Foundation (1902431), the NIHR (NIHR133761), and the Natural Sciences and Engineering Research Council of Canada, Discovery Grant (RGPIN-2023-05231). This work (AM) was partly supported by the Royal Society Wolfson Research Merit Award funded generously by the Wolfson Foundation. AM is a Distinguished Visiting Scholar to the Department of Mathematics, University of Johannesburg, South Africa, and the University of Pretoria in South Africa. MF and IS are members of the INdAM-GNCS activity group. The work of IS is supported by the PRIN 2020 research project (no. 2020F3NCPX) "Mathematics for Industry 4.0," and from the "National Centre for High Performance Computing, Big Data and Quantum Computing" funded by European Union – NextGenerationEU, PNRR project code CN00000013, CUP F83C22000740001.

CONFLICT OF INTEREST STATEMENT

The authors have no conflict of interest to declare.

DATA AVAILABILITY STATEMENT

All data are incorporated into the article.

ORCID

Massimo Frittelli https://orcid.org/0000-0002-1774-9320
Anotida Madzvamuse https://orcid.org/0000-0002-9511-8903

REFERENCES

[1] D. Adak, E. Natarajan, and S. Kumar, *Convergence analysis of virtual element methods for semilinear parabolic problems on polygonal meshes*, Numer. Methods Partial Differ. Equ. 35 (2019), no. 1, 222–245.
[2] R. A. Adams and J. F. Fournier, *Sobolev spaces*, Vol 140, Elsevier, Amsterdam, The Netherlands, 2003.
[3] B. Ahmad, A. Alsaedi, F. Brezzi, L. D. Marini, and A. Russo, *Equivalent projectors for virtual element methods*, Comput. Math. Appl. 66 (2013), no. 3, 376–391.
[4] P. F. Antonietti, L. Beirão Da Veiga, S. Scacchi, and M. Verani, *A C^1 virtual element method for the Cahn-Hilliard equation with polygonal meshes*, SIAM J. Numer. Anal. 54 (2016), no. 1, 34–56.
[5] E. Bachini, G. Manzini, and M. Putti, *Arbitrary-order intrinsic virtual element method for elliptic equations on surfaces*, Calcolo 58 (2021), 30.
[6] S. Bartels, C. Carstensen, and G. Dolzmann, *Inhomogeneous Dirichlet conditions in a priori and a posteriori finite element error analysis*, Numer. Math. 99 (2004), no. 1, 1–24.
[7] L. Beirão Da Veiga, F. Brezzi, A. Cangiani, G. Manzini, L. D. Marini, and A. Russo, *Basic principles of virtual element methods*, Math. Models Methods Appl. Sci. 23 (2013), no. 01, 199–214.
[8] L. Beirão Da Veiga, F. Brezzi, and L. D. Marini, *Virtual elements for linear elasticity problems*, SIAM J. Numer. Anal. 51 (2013), no. 2, 794–812.
[9] L. Beirão da Veiga, F. Brezzi, L. D. Marini, and A. Russo, *The Hitchhiker's guide to the virtual element method*, Math. Models Methods Appl. Sci. 24 (2014), no. 08, 1541–1573.
[10] L. Beirão Da Veiga, F. Dassi, and A. Russo, *High-order virtual element method on polyhedral meshes*, Comput. Math. Appl. 74 (2017), no. 5, 1110–1122.
[11] L. Beirão da Veiga, C. Lovadina, and A. Russo, *Stability analysis for the virtual element method*, Math. Models Methods Appl. Sci. 27 (2017), no. 13, 2557–2594.
[12] L. Beirão Da Veiga, C. Lovadina, and G. Vacca, *Divergence free virtual elements for the stokes problem on polygonal meshes*, ESAIM: M2AN 51 (2017), no. 2, 509–535.
[13] L. Beirão Da Veiga and G. Manzini, *A virtual element method with arbitrary regularity*, IMA J. Numer. Anal. 34 (2013), no. 2, 759–781.

[14] L. Beirão Da Veiga, A. Russo, and G. Vacca, *The virtual element method with curved edges*, ESAIM: M2AN 53 (2019), no. 2, 375–404.

[15] M. F. Benedetto, S. Berrone, and S. Scialò, *A globally conforming method for solving flow in discrete fracture networks using the virtual element method*, Finite Elem. Anal. Des. 109 (2016), 23–36.

[16] N. Benkemoun, A. Ibrahimbegovic, and J. B. Colliat, *Anisotropic constitutive model of plasticity capable of accounting for details of meso-structure of two-phase composite material*, Comput. Struct. 90 (2012), 153–162.

[17] S. Bertoluzza, M. Pennacchio, and D. Prada, *High order VEM on curved domains*, Atti Accad. Naz. Lincei Cl. Sci. Fis. Mat. Natur. 30 (2019), 391–412.

[18] S. Bianco, F. Tewes, L. Tajber, V. Caron, O. I. Corrigan, and A. M. Healy, *Bulk, surface properties and water uptake mechanisms of salt/acid amorphous composite systems*, Int. J. Pharm. 456 (2013), no. 1, 143–152.

[19] S. C. Brenner and L. Scott, *The mathematical theory of finite element methods*, Vol 3, Springer, New York, 2008.

[20] S. C. Brenner and L. Sung, *Virtual element methods on meshes with small edges or faces*, Math. Models Methods Appl. Sci. 28 (2018), no. 07, 1291–1336.

[21] F. Brezzi and L. D. Marini, *Virtual element methods for plate bending problems*, Comput. Methods Appl. Mech. Eng. 253 (2013), 455–462.

[22] E. Burman, P. Hansbo, M. Larson, and S. Zahedi, *Cut finite element methods for coupled bulk–surface problems*, Numer. Math. 133 (2016), no. 2, 203–231.

[23] A. Cangiani, E. H. Georgoulis, and S. Metcalfe, *Adaptive discontinuous Galerkin methods for nonstationary convection–diffusion problems*, IMA J. Numer. Anal. 34 (2014), no. 4, 1578–1597.

[24] J. Chen, *A memory efficient discontinuous Galerkin finite-element time-domain scheme for simulations of finite periodic structures*, Microw. Opt. Technol. Lett. 56 (2014), no. 8, 1929–1933.

[25] M. Chen and L. Ling, *Kernel-based meshless collocation methods for solving coupled bulk-surface partial differential equations*, J. Sci. Comput. 81 (2019), no. 1, 375–391.

[26] A. Y. Chernyshenko, M. A. Olshanskii, and Y. V. Vassilevski, *A hybrid finite volume–finite element method for bulk-surface coupled problems*, J. Comput. Phys. 352 (2018), 516–533.

[27] D. Cusseddu, L. Edelstein-Keshet, J. A. Mackenzie, S. Portet, and A. Madzvamuse, *A coupled bulk-surface model for cell polarisation*, J. Theor. Biol. 481 (2019), 119–135.

[28] K. Dai, G. Liu, and T. Nguyen, *An n-sided polygonal smoothed finite element method (nSFEM) for solid mechanics*, Finite Elem. Anal. Des. 43 (2007), no. 11, 847–860.

[29] F. Dassi, A. Fumagalli, A. Scotti, and G. Vacca, *Bend 3D mixed virtual element method for Darcy problems*, Comput. Math. Appl. 119 (2022), 1–12.

[30] A. Demlow, *Higher-order finite element methods and pointwise error estimates for elliptic problems on surfaces*, SIAM J. Numer. Anal. 47 (2009), no. 2, 805–827.

[31] E. Di Nezza, G. Palatucci, and E. Valdinoci, *Hitchhiker's guide to the fractional Sobolev spaces*, Bull. Sci. Math. 136 (2012), no. 5, 521–573.

[32] G. Dziuk and C. M. Elliott, *Finite element methods for surface PDEs*, Acta Numer. 22 (2013), 289–396.

[33] C. M. Elliott and T. Ranner, *Finite element analysis for a coupled bulk–surface partial differential equation*, IMA J. Numer. Anal. 33 (2013), no. 2, 377–402.

[34] C. M. Elliott, T. Ranner, and C. Venkataraman, *Coupled bulk-surface free boundary problems arising from a mathematical model of receptor-ligand dynamics*, SIAM J. Math. Anal. 49 (2017), no. 1, 360–397.

[35] M. Frittelli, A. Madzvamuse, and I. Sgura, *Bulk-surface virtual element method for systems of PDEs in two-space dimensions*, Numer. Math. 147 (2021), no. 2, 305–348.

[36] M. Frittelli, A. Madzvamuse, and I. Sgura, *The bulk-surface virtual element method for reaction-diffusion PDEs: analysis and applications*, Commun. Comput. Phys. 33 (2023), 733–763.

[37] M. Frittelli, A. Madzvamuse, I. Sgura, and C. Venkataraman, *Preserving invariance properties of reaction–diffusion systems on stationary surfaces*, IMA J. Numer. Anal. 39 (2017), no. 1, 235–270.

[38] M. Frittelli, A. Madzvamuse, I. Sgura, and C. Venkataraman, *Lumped finite elements for reaction–cross-diffusion systems on stationary surfaces*, Comput. Math. Appl. 74 (2017), no. 12, 3008–3023.

[39] M. Frittelli, A. Madzvamuse, I. Sgura, and C. Venkataraman, *Numerical preservation of velocity induced invariant regions for reaction–diffusion systems on evolving surfaces*, J. Sci. Comput. 77 (2018), no. 2, 971–1000.

[40] M. Frittelli and I. Sgura, *Virtual element method for the Laplace-Beltrami equation on surfaces*, ESAIM: M2AN 52 (2018), no. 3, 965–993.

[41] A. Fumagalli, A. Scotti, and L. Formaggia, "Performances of the mixed virtual element method on complex grids for underground flow," *Polyhedral methods in geosciences*, D. A. Di Pietro, L. Formaggia, and R. Masson (eds.), Springer, Cham, 2021, pp. 299–329.

[42] E. J. Fuselier and G. B. Wright, *A high-order kernel method for diffusion and reaction-diffusion equations on surfaces*, J. Sci. Comput. 56 (2013), no. 3, 535–565.

[43] F. Gardini, G. Manzini, and G. Vacca, *The nonconforming virtual element method for eigenvalue problems*, ESAIM Math. Model. Numer. Anal. 53 (2019), no. 3, 749–774.

[44] S. Gross, M. A. Olshanskii, and A. Reusken, *A trace finite element method for a class of coupled bulk-interface transport problems*, ESAIM: M2AN 49 (2015), no. 5, 1303–1330.

[45] B. Kovács and C. Lubich, *Numerical analysis of parabolic problems with dynamic boundary conditions*, IMA J. Numer. Anal. 37 (2017), no. 1, 1–39.
[46] D. Lacitignola, B. Bozzini, M. Frittelli, and I. Sgura, *Turing pattern formation on the sphere for a morphochemical reaction–diffusion model for electrodeposition*, Commun. Nonlinear Sci. Numer. Simul. 48 (2017), 484–508.
[47] D. Lacitignola, M. Frittelli, V. Cusimano, and A. De Gaetano, *Pattern formation on a growing oblate spheroid. An application to adult sea urchin development*, J. Comput. Dyn. 9 (2022), no. 2, 185–206.
[48] A. A. Lee, A. Münch, and E. Süli, *Degenerate mobilities in phase field models are insufficient to capture surface diffusion*, Appl. Phys. Lett. 107 (2015 Aug), no. 8, 081603.
[49] C. B. Macdonald, B. Merriman, and S. J. Ruuth, *Simple computation of reaction–diffusion processes on point clouds*, Proc. Natl. Acad. Sci. 110 (2013), no. 23, 9209–9214.
[50] J. A. Mackenzie, M. Nolan, and R. H. Insall, *Local modulation of chemoattractant concentrations by single cells: Dissection using a bulk-surface computational model*, Interface Focus 6 (2016), no. 5, 20160036.
[51] A. Madzvamuse and A. H. W. Chung, *The bulk-surface finite element method for reaction–diffusion systems on stationary volumes*, Finite Elem. Anal. Des. 108 (2016), 9–21.
[52] A. Madzvamuse, A. H. W. Chung, and C. Venkataraman, *Stability analysis and simulations of coupled bulk-surface reaction-diffusion systems*, Proc. R. Soc. A Math. Phys. Eng. Sci. 471 (2015), no. 2175, 20140546.
[53] L. Mascotto, I. Perugia, and A. Pichler, *A nonconforming Trefftz virtual element method for the Helmholtz problem: Numerical aspects*, Comput. Methods Appl. Mech. Eng. 347 (2019), 445–476.
[54] D. Mora, G. Rivera, and R. Rodríguez, *A virtual element method for the Steklov eigenvalue problem*, Math. Models Methods Appl. Sci. 25 (2015), no. 08, 1421–1445.
[55] F. Paquin-Lefebvre, W. Nagata, and M. J. Ward, *Pattern formation and oscillatory dynamics in a two-dimensional coupled bulk-surface reaction-diffusion system*, SIAM J. Appl. Dyn. Syst. 18 (2019), no. 3, 1334–1390.
[56] L. S. Ryder, Y. F. Dagdas, M. J. Kershaw, C. Venkataraman, A. Madzvamuse, et al., *A sensor kinase controls turgor-driven plant infection by the rice blast fungus*, Nature 574 (2019), no. 7778, 423–427.
[57] S. L. Sobolev, *Partial differential equations of mathematical physics*, Elsevier, Amsterdam, The Netherlands, 1964.
[58] E. M. Stein, *Singular integrals and differentiability properties of functions (PMS-30)*, Princeton University Press, Princeton, NJ, 1971.
[59] G. Vacca, *Virtual element methods for hyperbolic problems on polygonal meshes*, Comput. Math. Appl. 74 (2016), no. 5, 882–898.
[60] G. Vacca and L. Beirão Da Veiga, *Virtual element methods for parabolic problems on polygonal meshes*, Numer. Methods Partial Differ. Equ. 31 (2015), no. 6, 2110–2134.

How to cite this article: M. Frittelli, A. Madzvamuse, and I. Sgura, *Virtual element method for elliptic bulk-surface PDEs in three space dimensions*, Numer. Methods Partial Differ. Eq. (2023), 1–27. https://doi.org/10.1002/num.23040

APPENDIX A: PRELIMINARY DEFINITIONS AND RESULTS

In this appendix, we provide preliminary definitions, results and notations adopted throughout the article. Unless explicitly stated, definitions and results are taken from [32].

A.1 | Surfaces and differential operators on surfaces

Let $\Omega \subset \mathbb{R}^3$ be a compact set such that its boundary $\Gamma := \partial\Omega \subset \mathbb{R}^3$ is a $\mathcal{C}^k$, $k \geq 2$ surface. Since Γ can be seen as the zero level set of the *oriented distance function* $d : \mathbb{R}^3 \to \mathbb{R}$ defined by

$$d(\boldsymbol{x}) := \begin{cases} -\inf\{\|\boldsymbol{x}-\boldsymbol{y}\| : \boldsymbol{y} \in \Gamma\} & \text{if } \boldsymbol{x} \in \Omega; \\ 0 & \text{if } \boldsymbol{x} \in \Gamma; \\ \inf\{\|\boldsymbol{x}-\boldsymbol{y}\| : \boldsymbol{y} \in \Gamma\} & \text{if } \boldsymbol{x} \in \mathbb{R}^3 \setminus \Omega, \end{cases}$$

then the outward unit vector field $\boldsymbol{\nu} : \Gamma \to \mathbb{R}^3$ can be defined by

$$\boldsymbol{\nu}(\boldsymbol{x}) := \frac{\nabla d(\boldsymbol{x})}{\|\nabla d(\boldsymbol{x})\|}, \qquad \boldsymbol{x} \in \Gamma. \tag{A1}$$

Lemma 5 (Fermi coordinates [32]). *If Γ is a C^k, $k \geq 2$ surface, there exists an open neighborhood $U \subset \mathbb{R}^3$ of Γ such that every $\boldsymbol{x} \in U$ admits a unique decomposition of the form $\boldsymbol{x} = \boldsymbol{a}(\boldsymbol{x}) + d(\boldsymbol{x})\boldsymbol{\nu}(\boldsymbol{a}(\boldsymbol{x}))$, $\boldsymbol{a}(\boldsymbol{x}) \in \Gamma$. The maximal open set U with this property is called the Fermi stripe of Γ (see Figure 1a), $\boldsymbol{a}(\boldsymbol{x})$ is called the normal projection onto Γ and $(\boldsymbol{a}(\boldsymbol{x}), d(\boldsymbol{x}))$ are called the Fermi coordinates of $\boldsymbol{x}$. The oriented distance function fulfils $d \in C^k(U)$.*

Definition 6 ($C^1(\Gamma)$ functions). A function $u : \Gamma \to \mathbb{R}$ is said to be $C^1(\Gamma)$ if there exist an open neighborhood U of Γ and a C^1 function $\hat{u} : U \to \mathbb{R}$ such that $\hat{u}_{|\Gamma} = u$, that is, $\hat{u}$ is a C^1 extension of u off Γ.

Definition 7 (Tangential gradient and tangential derivatives). The tangential gradient $\nabla_\Gamma u$ of a function $u \in C^1(\Gamma)$ is defined by $\nabla_\Gamma u(\boldsymbol{x}) := \nabla \hat{u}(\boldsymbol{x}) - (\nabla \hat{u}(\boldsymbol{x}) \cdot \boldsymbol{\nu}(\boldsymbol{x}))\boldsymbol{\nu}(\boldsymbol{x})$ for all $\boldsymbol{x} \in \Gamma$. The result of the computation of $\nabla_\Gamma u$ is independent of the choice of the extension $\hat{u}$. The components $D_x u$, $D_y u$, and $D_z u$ of the tangential gradient $\nabla_\Gamma u$ are called the tangential derivatives of u.

Definition 8 ($C^k(\Gamma)$ functions). For $k \in \mathbb{N}$, $k > 1$, a function $u : \Gamma \to \mathbb{R}$ is said to be $C^k(\Gamma)$ if it is $C^1(\Gamma)$ and its tangential derivatives are $C^{k-1}(\Gamma)$.

Definition 9 (Laplace–Beltrami operator). The Laplace–Beltrami $\Delta_\Gamma u$ of a function $u \in C^2(\Gamma)$ is defined by $\Delta_\Gamma u(\boldsymbol{x}) := D_x D_x u(\boldsymbol{x}) + D_y D_y u(\boldsymbol{x})$ for all $\boldsymbol{x} \in \Gamma$.

A.2 | Bulk- and surface function spaces

Throughout the article, we will adopt the following notations. For $p \in [1, +\infty]$, $L^p(\Omega)$ and $L^p(\Gamma)$ denote the usual Lebesgue spaces on Ω and Γ, respectively, with $\|\cdot\|_{L^p(\Omega)}$ and $\|\cdot\|_{L^p(\Gamma)}$ being the respective norms. For $m \in (0, +\infty)$ and $p \in [1, +\infty]$, $W^{m,p}(\Omega)$ and $W^{m,p}(\Gamma)$ denote the (possibly fractional) Sobolev spaces of order m on Ω and Γ, respectively, with $\|\cdot\|_{W^{m,p}(\Omega)}$ and $\|\cdot\|_{W^{m,p}(\Gamma)}$ being the respective norms. Full definitions can be found in [35].

Lemma 6 (Inclusion between fractional Sobolev spaces [31]). *Let $\Omega \subset \mathbb{R}^3$ be a bounded domain with a C^1 boundary Γ, let $p \in [1, +\infty)$ and $s, s' \in [0, +\infty)$ such that $s < s'$. Then there exists a constant $C > 0$ depending on Ω and s such that*

$$\|u\|_{W^{s,p}(\Omega)} \leq C \|u\|_{W^{s',p}(\Omega)}, \tag{A2}$$

for all $u \in W^{s',p}(\Omega)$. Hence, $W^{s,p}(\Omega) \subset W^{s',p}(\Omega)$.

A.3 | Fundamental results in bulk- and surface calculus

Theorem 5 (Narrow band trace inequality [33]). *With the notations of the previous theorem, there exists $C > 0$ depending on Ω such that any $u \in H^1(\Omega)$ fulfils*

$$\|u\|_{L^2(U_\varepsilon)} \leq C \varepsilon^{\frac{1}{2}} \|u\|_{H^1(\Omega)}. \tag{A3}$$

Theorem 6 (Trace theorem and inverse trace theorem [57, 58]). *Let $k \in \mathbb{N}$, $\frac{1}{2} < s \leq k$ and assume that the boundary Γ is a C^k surface.*[2] *Then there exists a bounded operator*

[2]It is sufficient that Γ be a $C^{k-1,1}$ surface, meaning that its derivatives up to order $k-1$ are Lipschitz continuous. For simplicity, we use the stronger assumption that $\Gamma \in C^k$.

$\mathrm{Tr} : H^s(\Omega) \to H^{s-\frac{1}{2}}(\Gamma)$, *called the trace operator, such that* $\mathrm{Tr}(u) = u_{|\Gamma}$ *and*

$$\|\mathrm{Tr}(u)\|_{H^{s-\frac{1}{2}}(\Gamma)} \leq C\|u\|_{H^s(\Omega)}, \qquad \forall\, u \in H^s(\Omega). \tag{A4}$$

The trace operator has a continuous inverse operator $\mathrm{Tr}^{-1} : H^{s-\frac{1}{2}}(\Gamma) \to H^s(\Omega)$ *called Babič inverse such that*

$$\|\mathrm{Tr}^{-1}(v)\|_{H^s(\Omega)} \leq C\|v\|_{H^{s-\frac{1}{2}}(\Gamma)}, \qquad \forall\, v \in H^{s-\frac{1}{2}}(\Gamma). \tag{A5}$$

Theorem 7 (Sobolev extension theorem [58])**.** *Assume that* $\Omega \subset \mathbb{R}^3$ *has a Lipschitz boundary* Γ, *let* $r \in \mathbb{N}$ *and* $p \in [1, +\infty]$. *Then, for any function* $u \in W^{r,p}(\Omega)$, *there exists an extension* $\widetilde{u} \in W^{r,p}(\mathbb{R}^3)$ *such that* $\widetilde{u}_{|\Omega} = u$ *and*

$$\|\widetilde{u}\|_{W^{r,p}(\mathbb{R}^3)} \leq C\|u\|_{W^{r,p}(\Omega)}, \tag{A6}$$

where $C > 0$ *depends on* Ω *and* r, *but not on* p.

Theorem 8 (Sobolev embeddings)**.** *Let* $d \in \mathbb{N}$, $d \geq 2$ *be a number of dimensions and assume that* $\Omega \subset \mathbb{R}^d$ *has a Lipschitz boundary*.

- *If* $0 < \gamma < 1$, *then* $H^{d/2+\gamma}(\Omega) \hookrightarrow C^{0,\gamma}(\Omega)$ *is a continuous embedding, hence* $\|u\|_{C^{0,\gamma}(\Omega)} \leq C_\gamma \|u\|_{H^{d/2+\gamma}(\Omega)}$. *From the definition of the Hölder space* $C^{0,\gamma}(\Omega)$ *we have that*

$$\|u(\boldsymbol{x}) - u(\boldsymbol{y})\| \leq C_\gamma \|u\|_{H^{d/2+\gamma}(\Omega)} \|\boldsymbol{x} - \boldsymbol{y}\|^\gamma, \qquad \text{a.e. } (\boldsymbol{x}, \boldsymbol{y}) \in \Omega \times \Omega. \tag{A7}$$

- *If* $\varepsilon > 0$, *then* $H^{d/2+\varepsilon}(\Omega) \hookrightarrow C(\Omega)$ *is a continuous embedding*.

Proof. See [2] for the case of integer-order Sobolev spaces and [31] for the fractional case. ∎